JCSE The Journal of Corrosion Science and Engineering

Century 21st Corrosion Science

Volume 6 Paper C059

Corrosion Studies of Duplex Stainless Steels with Micrometer Resolution

M. Femenia, J. Pan, and C. Leygraf

Division of Corrosion Science
Department of Materials Science and Engineering
Royal Institute of Technology
SE- 100 44 Stockholm, Sweden

Abstract

The local corrosion behavior of duplex stainless steel (DSS) is affected by a wide variety of factors. Localized corrosion of DSS frequently starts at micrometer scale inclusions or precipitates, which are often segregated in the austenite-ferrite boundary regions. Moreover, due to the partitioning of the key alloying elements of ferrite (Cr and Mo) and austenite (N and Ni), the local interactions between the phases must also be considered.

The aim of this doctoral study was to increase the knowledge about the local dissolution behavior of DSS in acidic-chloride environments. The recent developments of new local probing techniques have opened a new frontier in corrosion science, providing valuable local information not accessible in the past. The local techniques used include electrochemical scanning tunneling microscopy (EC-STM), scanning probe force microscopy (SKPFM), magnetic force microscopy (MFM), and scanning Auger electron Spectroscopy (SAES), all with micrometer or sub-micrometer resolution.

With EC-STM, it was possible to monitor local dissolution processes on DSS *in situ*, and in real time. MFM was capable of imaging the phase distribution in DSS without the need of the traditional surface etching, while SKPFM revealed that the Volta potential difference between the two phases was measurable and significant. SAES showed that the composition gradient at the phase boundaries is narrower than 2 μm.

Different types of DSSs have been studied, from low-alloyed DSS to superduplex. Higher contents of Cr, Mo and N strengthened both phases as well as the phase boundaries, resulting in phases having similar corrosion resistance that showed a more uniform dissolution behavior. However, the Volta potential difference between the phases proved to be of the same order for all the DSSs studied. Austenite was in general associated to regions

This is an unrefereed preprint, and it should not be referenced. The refereed paper will appear in the Journal of Corrosion Science and Engineering at http://www.umist.ac.uk/corrosion/jcse

This paper was presented at the Conference "Corrosion Science in the 21st Century" held at UMIST in July 2003.

displaying a more noble Volta potential than ferrite, resulting in a higher dissolution rate of the ferrite next to the austenite phase.

1. INTRODUCTION

In the early 20th century, simultaneous research in USA, England and Germany lead to the development of stainless steel. Monnard and Strauss in Germany, and Brearley in England are often regarded as three of the most important pioneers.[1, 2, 3] The first two-phase microstructure was reported by Bain and Griffiths in 1927,[4, 5] and shortly afterwards the first duplex stainless steels (DSSs) were already commercially available.[6] However, it was not until the 1980's, when the advent of AOD (Argon-oxygen decarburization) allowed the fabrication of low-carbon stainless steels, that DSS found widespread industrial application.[7]

A steel is considered to be stainless when it contains more than 12% Cr,* which makes possible the formation of a protective Cr-based passive film on the surface. DSS is composed of two phases that are stainless, and present in relatively large separate volumes and in approximately equal volume fractions.[4, 5] The term DSS has become a synonym for the ferritic-austenitic steels due to their extensive use in industrial applications, although it technically also comprises other types of steels, such as the ferritic-martensitic.

DSS solidifies as ferrite, part of which transforms to austenite during subsequent cooling, yielding the prescribed mix of the two phases at room temperature.[8] The exact volume fraction of each phase depends on the alloying composition and the heat treatment. However, most alloys are designed to contain similar amounts of each phase at room temperature.

Due to its small grain size, DSS possesses higher yield strength than both ferritic and austenitic stainless steel. However, it is not the attractive mechanical properties that have increased the interest for DSS in the past two decades, but the superior corrosion resistance, especially in chloride-containing environments, compared to austenitic steel of comparable cost.[4, 5] Thus, DSS has been increasingly used in marine environments, and in oil and gas, pulp and paper, chemical, petrochemical, and power industries. [4, 5, 8] This type of environments

* All compositions in this study are in wt%, unless noted

pose a challenge in terms of localized corrosion resistance, which has become one of the most important issues for DSS. The resistance to localized corrosion is strongly dependent on the chemical composition of the steel,[4] Cr, Mo, and N being the most beneficial alloying elements.

Localized corrosion often starts at small sites such as inclusions, precipitates, or cracks that can be on a micrometer or sub-micrometer scale. Thus, the size and distribution of precipitates and inclusions in the microstructure may play a crucial role in the corrosion resistance of the material.[9] This is especially important in the case of DSS, because the duplex structure introduces anomalies in the distribution of impurities and precipitates, and as a result, phase boundaries frequently become preferential sites for the segregation of impurities or precipitations. [4, 5, 8] Moreover, the partitioning of the alloying elements between the phases (Cr and Mo partition to ferrite, and N and Ni to austenite) [4, 5, 8, 10-18] further complicates the corrosion behavior of DSS, since local interactions between the phases must also be taken into account.[10, 14-16] Consequently, it is easy to realize that a deeper knowledge of the local electrochemical activity and the corrosion processes taking place on micrometer and sub-micrometer scales would help to improve the understanding of the mechanisms behind localized corrosion, leading to the development of better stainless steels.

Corrosion studies often involve the application of conventional electrochemical techniques (potentiostatic, potentiodynamic, impedance, etc.) followed by subsequent *ex situ* characterization by means of optical microscopy, scanning electron microscopy (SEM) or surface analysis. These electrochemical methods are usually based on exposed electrode areas of the order of one cm^2, and are therefore not capable of providing direct information about the local corrosion processes taking place on the sample. However, during the last decade or so, numerous high-resolution experimental techniques have been developed for corrosion studies, and many of them permit the characterization of the solid-liquid interface *in situ*.

Techniques used for local *in situ* studies of corrosion of stainless steels include microelectrodes,[19] microcells,[18, 20, 21] localized electrochemical impedance spectroscopy (LEIS),[22, 23] scanning vibrating electrode technique (SVET)[24], scanning reference electrode technique (SRET),[25, 26] scanning tunneling microscopy (STM),[27, 28] atomic force microscopy (AFM),[29-33] scanning electrochemical microscopy (SECM),[34-38] and scanning Kelvin probe (SKP).[39-41] Combinations of these techniques have also been reported.[42-45] The SRET and SVET techniques are capable of mapping the current density over the surface of the electrode, and of distinguishing local potential differences with a lateral resolution of a few tens of micrometers. The AFM/STM techniques can monitor changes in topography (3D) of the

sample with sub-micron resolution. The SECM technique can provide information about surface species present, or map the local faradaic current over the surface of the sample, also with sub-micron resolution. The SKP technique measures the Volta potential variation over the surface of the electrode under a thin electrolyte layer with a resolution of 50-100 μm. An AFM-based variation of this technique, scanning Kelvin probe force microscopy (SKPFM), has recently been applied to corrosion studies,[46-50] but, to our knowledge, nothing has yet been reported on stainless steel. The main advantage of this technique over the standard SKP is its high lateral resolution (in the sub-micron range), but the problem is that it cannot be used *in situ*. In all, the information that can be obtained with local techniques is quite comprehensive, and a combination of such techniques might be of invaluable importance for gaining additional knowledge about corrosion processes.

Acidic-chloride environments are present in many commercial applications of DSS, such as marine environments or chloride-bearing pressure vessels. Moreover, in localized corrosion processes such as pitting and crevice corrosion, local environments inside the pits or crevices often become acidified and enriched in chloride ions. Therefore, it seemed a highly relevant medium in which to study the local corrosion behavior of DSS.

The primary aim of this project was to gain deeper understanding of the local processes -electrochemical, chemical or physical- that may affect the corrosion resistance of DSS in acidic-chloride environments. These processes are of vital importance for the dissolution, passivation, and localized corrosion behavior of DSS, because they influence the level of performance of these steels in real-life applications. Hence, there are obvious technical and industrial interests; this project was implemented as a collaboration with our industrial partners, AB Sandvik Steel and Avesta Polarit AB, in January 1998. An important prerequisite was also the joint decision made by KTH and the Swedish Institute for Metals Research, Stockholm, to purchase an AFM and a modification package for electrochemical STM and SECM facilities to be shared by both parts.

2. EXPERIMENTAL

2.1 Materials and Solutions

In the course of these studies, four different DSSs were investigated: 2205 (Ref. 82), UNS S32750 (Refs. 82-86), UNS S32304 (Refs. 84-86), and UNS S31803 (Refs. 84-86). From Table I it is possible to see that these steels present a broad variation of alloying elemental concentrations, ranging from the low-alloyed UNS S32304 to the super duplex UNS S32750. The 2205 DSS in Ref. 82 was a commercial alloy, with the same nominal composition as UNS S31803, that had undergone a heat treatment in order to obtain a coarser grain size (10-30 μm). For the other three steels, no further heat treatment was needed because of the high resolution offered by the EC-STM.

Table I. Chemical composition of the DSSs investigated (wt%).[*]

Steel	Cr	Ni	Mo	N	C	Si	Mn	P	S
UNS S32304	22.7	4.78	0.21	0.10	0.020	0.36	1.48	0.022	0.001
2205	22.1	5.59	2.99	0.13	0.025	0.41	1.51	0.020	0.001
UNS S31803	22.0	5.36	3.20	0.17	0.015	0.50	0.78	0.003	0.001
UNS S32750	24.8	6.95	3.84	0.27	0.014	0.27	0.44	0.003	0.001

These steels are commercially available and widely used in industrial applications where high mechanical and corrosion resistance are needed. Important applications include heat exchangers, refineries, and process systems in oil and gas industries. The steels belong to the modern generation of low-carbon DSSs that have been designed so that the austenite re-formation in the heat-affected zone adjacent to the weld occurs quickly, yielding welded joints with good mechanical and corrosion properties.[51] In addition, UNS S32750 undergoes a solution treatment that leads to equal PRE[†] values for the austenite and ferrite.[44]

The choice of acidic-chloride solutions was based on the relevance of this medium in many commercial applications of DSS. In Ref. 82, two solutions were used; a 0.05 M H_2S0_4 +

[*] UNS S32304, UNS S31803, and UNS S32750 were supplied by AB Sandvik Steel AB Sandvik Steel, and 2205 was supplied by Avesta Polarit AB.
[†] Pitting Resistance Equivalent, PRE = %Cr + 3.3 %Mo + *k* %N, where $10<k<30$.

1M NaCl in order to simulate a relatively mild environment, and a 4M H_2S0_4 + 1M HCl solution (also used in Ref. 83) for simulating aggressive environments, or the type of solution that might be found inside pits or crevices. In Refs. 85 and 86, 1M H_2SO_4 + 1M NaCl was chosen because the polarization curves of the three DSSs investigated showed clear active peaks, and it was not too aggressive for the lower-alloyed steels.

2.2 Conventional Electrochemical Techniques

In parallel to the local measurements, conventional potentiostatic and potentiodynamic measurements were carried out in order to characterize the global behavior of the different materials in the solutions tested. Potentiostatic experiments are used for assessing the corrosion behavior of a sample at a given potential. In this type of measurements, a potential is applied to the sample and held constant, while the resulting current is measured as a function of time (e.g. Figure 4, Ref. 82). On the other hand, potentiodynamic measurements show the behavior of the sample over a whole range of potentials (e.g. Figure 3, Ref. 82). In this case, the potential is swept at a fixed sweep rate, while the resulting current is measured continuously. In these studies, the sweep was started at cathodic potentials (i.e., negative to the open-circuit potential) and increased until a preset limit was reached. The sweep rate is an important parameter in potentiodynamic polarization measurements, because it influences the resulting current. Slower sweep rates yield usually lower current values at all potentials of the polarization curve, especially in the passive region.[52] In this work, all potentiodynamic measurements were carried out with a sweep rate of 20 mV/min.

The conventional electrochemical experiments were performed using an EG&G 273A Potentiostat-Galvanostat system controlled by a Model 352 Corrosion Software. The electrochemical cell used represented a standard three-electrode configuration, with a Pt counter electrode and an Ag/AgCl reference electrode.

2.3 Electrochemical Scanning Tunneling Microscopy and Scanning Electrochemical Microscopy

The instrument used for the main body of EC-STM measurements was originally an AFM (Quesant Resolver). Modifications of this instrument permitting STM and SECM

measurements had been reported in literature, for which it seemed an optimal choice.[36-38] The AFM scanning-head was replaced by another head modified for STM and SECM measurements, and controlled by an additional control unit and software. The advantage of this set-up is that STM and SECM measurements can be performed on the same area and with the same tip by just switching some software parameters. The change of the instrumental mode can even be performed *in situ* during the course of an experiment, which permits an easy combination of the two techniques.

The system was placed inside a steel-cased refrigerator standing on thick rubber plates. This configuration isolates the system from electrical and acoustic noise as well as from thermal variations and mechanical vibrations, for which all scanning probe microscopy (SPM) systems are very sensitive. The electrochemical cell for the EC-STM and SECM experiments had a two-electrode configuration. The working electrode (~1 mm^2) is completely surrounded by the much larger Pt counter electrode (~5 cm^2), which also acts a pseudo-reference electrode (Figure 1). The potential stability of the Pt counter electrode in this kind of solutions was checked through open-circuit potential measurements against a standard Ag/AgCl reference electrode, as well as through potentiodynamic measurements in a three-electrode cell configuration (with glassy carbon as counter electrode, and the Pt as working electrode). The results were considered satisfactory and legitimated the use of Pt as pseudo reference electrode in the EC-STM experiments.

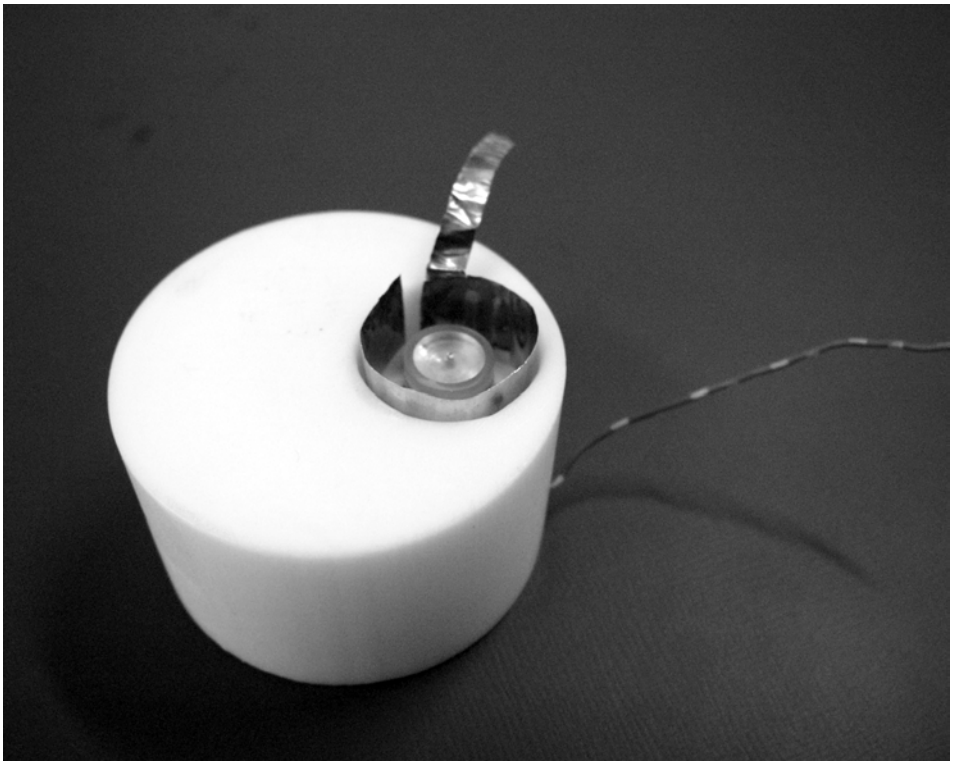

Figure 1. EC-STM/SECM cell configuration.

In this system, the tip is electrically connected to the counter electrode, therefore, the bias voltage between the tip and the surface is equal to the potential difference between the working and counter electrodes. The bias voltage is regulated through the software and controlled by the additional control unit.

The tips were made from a Ø 0.25 mm Pt-20%Ir wire. The wire was first cut and soldered to a tip holder, after which it was electrochemically etched in a saturated $CaCl_2$ solution by applying 30 V AC. The tip could be sharpened further by etching it in a saturated $NaHSO_4$ solution and applying 7 V AC. After the sharpening process, the tip was insulated with lacquer so that only the very end was exposed to solution.

2.3.1 Scanning Tunneling Microscopy

STM is based on quantum mechanical tunneling, a phenomenon that occurs when electrons pass between solids without having to cross an activation energy barrier.[53] In STM, tunneling occurs when a sharp conductive tip is brought close enough (0.3-1 nm) to a conducting surface, and a bias voltage is applied between them.[54, 55] The topographic information is obtained when the tip is scanned over the surface of the sample and a feedback circuit adjusts the vertical position of the tip, so that the tunneling current (and therefore the tip-sample distance) is maintained constant (Figure 2a).

In the EC-STM experiments the cell was filled with solution so that the sample surface was covered by a solution layer approximately 3 mm thick. Then, the sample was left one hour in order to allow the stabilization of E_{corr}, which was measured and entered in the software as the bias voltage. After connecting the cell to the STM system, the imaging of the surface could begin. The samples were imaged from E_{corr} to higher anodic potentials, acquiring three images at each potential. Since the acquisition time for each image was 5 minutes, the sample was held 15 minutes at each potential.

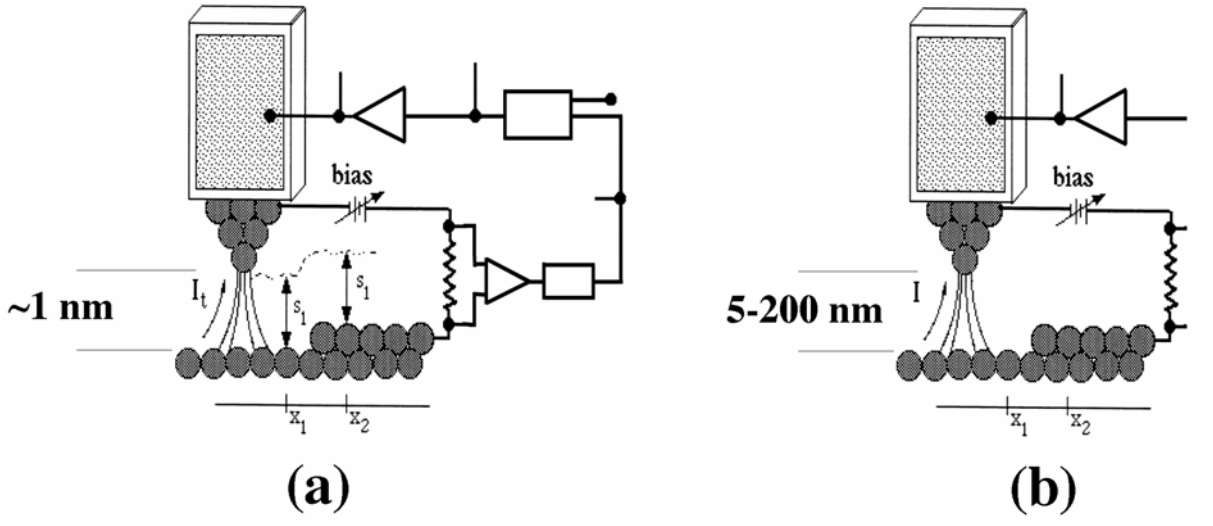

Figure 2. Diagram of the working principle of (a) STM and (b) SECM.

2.3.2 Scanning Electrochemical Microscopy

In SECM, an ultramicroelectrode tip is scanned over the surface of the sample, and the current collected can be used in a variety of ways. In fact, almost any type of electrochemical measurement can be performed with SECM, with the advantage of a greatly improved lateral resolution.[34, 56]

In this system, the tip is electrically connected to the counter electrode so that it is possible to image, with sub-micron resolution, the electrochemical current originating from the local corrosion processes taking place on the electrode surface. Another advantage of this set up is that the current signals from both the tip and the large counter electrode are recorded. Hence, it is possible to simultaneously obtain both local and global information about the electrochemical activity of the sample.

The SECM experiments were usually performed in combination with EC-STM measurements by just changing the instrument mode in the software. This disabled the feedback system (Figure 2b), which had the advantage of making possible higher scan rates. In SECM mode, the acquisition time for each image was only 30 seconds.

2.4 Ex situ Microstructure Characterization

EC-STM provides very interesting information about the corrosion processes taking place on a local scale, but its ability to estimate the global corrosion behavior of the sample is limited. Therefore, it is important to characterize the sample by complementary techniques after the *in situ* experiments have been finished. Subsequent *ex situ* characterization of the sample not only permits a more certain identification of the phases, but also yields complementary information about the processes that might have taken place on the overall surface during the experiment. This information can then be used as a link between the global information given by the conventional electrochemical techniques and the local information yielded by EC-STM.

After the EC-STM experiments, the sample was investigated by means of optical microscopy and SEM in order to identify the phases observed and to confirm the observations made during the local experiments. Samples that had undergone potentiodynamic polarization were also characterized *ex situ* for comparison with the samples that had been used for EC-STM. The microstructure of non-exposed samples was used as a reference for these characterizations.

2.5 Magnetic Force Microscopy and Scanning Kelvin Probe Force Microscopy

The MFM and SKPFM measurements in Ref. 85 were performed with a commercial AFM, MultiMode™ Nanoscope IV (Digital Instruments) located at the Division of Nanostructure Physics, Royal Institute of Technology, KTH. The versatility of this instrument allows, in a two-pass procedure, to measure a second signal in addition to AFM surface topography. For MFM and SKPFM measurements, this is possible by using CoCr-coated tips. This set-up allows a very easy combination of the two techniques by simply changing some software parameters.

2.5.1 Magnetic Force Microscopy

MFM is a member of the large family of SPMs derived from the invention of STM. In MFM, the magnetic fields adjacent to a sample are detected with sub-micron resolution by scanning a magnetic probe over the surface and recording the changes in its phase or resonant

frequency.[57] In these studies, the CoCr-coated tip was magnetized in the direction perpendicular to the sample surface.

Once set in place in the instrument, the tip is oscillated at its resonant frequency by a piezoelectric element, and scanned over the sample surface. The topography of the sample surface is obtained in the first pass by lightly tapping the surface with the tip. In the second pass, the tip is lifted off the surface by a predetermined distance (in this work, between 50 and 100 nm) so that only the magnetic forces affect the tip, thus avoiding interference from the surface topography.[57-59] Then, the tip is scanned along the same line following the topographic surface contour recorded during the first pass, so that the tip-sample distance, and hence the resolution, are maintained constant. In this way, the phase shift induced by the magnetic force gradient between the tip and the sample can be recorded, yielding an image of the magnetic patterns over the surface, which in the case of DSS can be associated to the microstructure of the sample (see Figure 3).

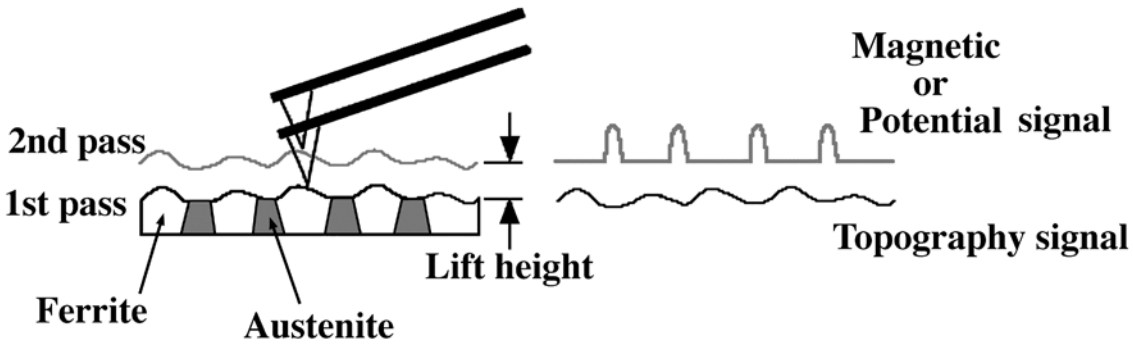

Figure 3. Diagram of the working principle of MFM and SKPFM.

2.5.2 Scanning Kelvin Probe Force Microscopy

The Kelvin probe is a technique generally used to measure the Volta potential of metals in vacuum or in gases.[60] Its application to corrosion studies dates from the late 80's, when Stratmann demonstrated a linear relationship between the Volta potential measured on an electrode under a thin electrolyte layer and its corrosion potential (E_{corr}) in that solution.[39, 61-63] Approximately one decade later, SKPFM (another SPM technique) found applications to corrosion science.[46-50] Although SKPFM and SKP are fundamentally different techniques,

Frankel *et al.* proved that the signal measured by SKPFM on an emersed electrode can also be related to its E_{corr} in that solution.[46, 48] However, the interpretation of the measured Volta potential is not straightforward, since it is difficult to relate the Volta potential measured in air to the E_{corr} measured in solution because of their different physical origins. In these studies, the focus has been on using the Volta potential variation as a qualitative measure of the practical nobility, rather than trying to obtain absolute values for quantitative evaluations of the corrosion processes.

In the SKPFM measurements, the topography of the sample is obtained in the first pass, as described above for MFM. In the second pass, however, the tip is lifted 100 nm so that it is placed in the region where the Volta potential is independent of the tip-sample distance,[46, 48] which also prevents the interference of topographic features on the potential image.[64] In this case, the mechanical oscillation of the tip is suppressed by turning off the piezoelectric element that usually drives it, and instead an oscillating AC voltage (± 3V) is applied to the tip. Consequently, if there is a potential difference between the tip and the sample (V_{ts}), an oscillating electric force will act on the tip, causing it to vibrate. If a DC voltage equal in magnitude (but opposite in sign) to V_{ts} is applied to the tip, the potential difference will be cancelled and the tip will stop oscillating. This DC voltage is then recorded and used to construct a map of the surface potential. Since this is a nulling technique, the output signal from the instrument needs to be inverted in order to obtain the right polarity of the potential measured. The potential values obtained are referred to the tip, and since its potential may vary with changes in the metal coating, it cannot be used as an absolute reference electrode. [46, 48, 65] Therefore, the values obtained can only be used to make quantitative comparisons within the same image.

The main disadvantage of this technique is that the large voltages applied to the tip do not permit measurements in aqueous environments, because they would trigger electrochemical reactions. Thus, all SKPFM measurements presented in this study were carried out in air.

2.6 Scanning Auger Electron Spectroscopy

In SAES, the sample is bombarded by an electron beam that ejects electrons from a core level of the surface atoms. The core hole is then filled by an electron from a higher energy level. The energy liberated by this de-excitation is taken by a third electron, which is

ejected from the atom with a characteristic energy. The ejected electron, known as Auger electron, is surface specific, giving chemical information only from the outermost atom layers.[66]

The equipment used in these studies was a Perkin-Elmer Physical Electronics PHI 590, located at the Department of Physics, Chalmers University of Technology in Gothenburg. The primary beam energy used was 3 kV, with a primary electron beam current of 50 nA, which yielded a spot size (resolution) of approximately 1 μm. The electron gun bombarded the surface at 45°. In order to remove surface contamination, an Ar^+ gun was operated at 3 kV with a beam current of 0.5 μA.

Before the measurements, a sputter depth profile was obtained for each sample by sputtering a region of approximately 1 x 1 mm until the oxygen signal had completely disappeared. In this way, it was possible to determine the thickness of the oxide film, considered to be the sputter depth at which the concentration of oxygen drops to half of its value at the surface.[67] The time needed to sputter away the air-formed oxide film was noted, and another region of the sample was sputtered during the same amount of time. In this way, the subsequent SAES measurements could be performed on the surface alloy layer at the oxide/metal interface.

The results from the SAES measurements presented in this work consist of concentration line-profiles for Cr, Ni, Mo and N obtained across the ferrite-austenite phase boundary. The line-profiles performed were 12 μm long, containing 30 measuring points evenly spaced every 0.4 μm. The measuring time for each line-profile was approximately one hour. In order to decrease the statistic uncertainty, the line-profile measurements were repeated three times for each sample and their result was averaged. Due to background noise, the line-profiles of some elements with low concentration (N and Mo for UNS S32304, and N for UNS S31803), yielded negative concentration values despite the fact that the difference in concentration of the element between the phases was detectable.

3. SUMMARY OF RESULTS

3.1 Electrochemical Scanning Tunneling Microscopy

3.1.1 UNS S32750 and 2205 in 4M H_2S0_4 + 1M HCl

The dissolution behavior of a coarse-grained 2205 DSS (Ref. 82) and of UNS S32750 (Ref. 83) was investigated in 4M H_2S0_4 + 1M HCl. The main difference in composition between these steels lies in their Cr, Mo and N contents (see Table I). It is known that the addition of these elements to stainless steels depresses active dissolution and reduces the passive current density.[68] In this solution, however, the effect of the alloying elements in the active potential region could not be discerned when comparing their potentiodynamic polarization curves (Figure 1, Ref. 83).

The EC-STM measurements, however, revealed that the two steels exhibited a very different local dissolution behavior. The 2205 showed selective dissolution of the ferrite phase as the potential was increased to anodic values. Before the experiments, the sample was immersed in the solution during one hour in order to allow for the stabilization of E_{corr}. The surface appeared quite smooth, and no phases were distinguishable from the EC-STM image (Figure 4a). At low anodic potentials (E_{corr} + 50 mV), ferrite dissolved selectively, while austenite seemed to remain virtually unchanged (Figure 4b). At higher anodic potentials (E_{corr} + 150 mV), stepwise dissolution at the austenite edges could be discerned, while ferrite seemed to be still dissolving at a higher rate than austenite, as judged from the continuous increase of the z-scale between the two phases (Figure 4c). Increasing the potential further to E_{corr} + 180 mV caused an increase in the dissolution rate of the austenite, but still it seemed to remain lower than that of ferrite. The z-scale difference between the two phases reached approximately 5 μm, with sharp edges at the phase boundaries. A remarkable observation was that the ferrite at the phase boundary region seemed to dissolve at a greater rate than the ferrite in the bulk.

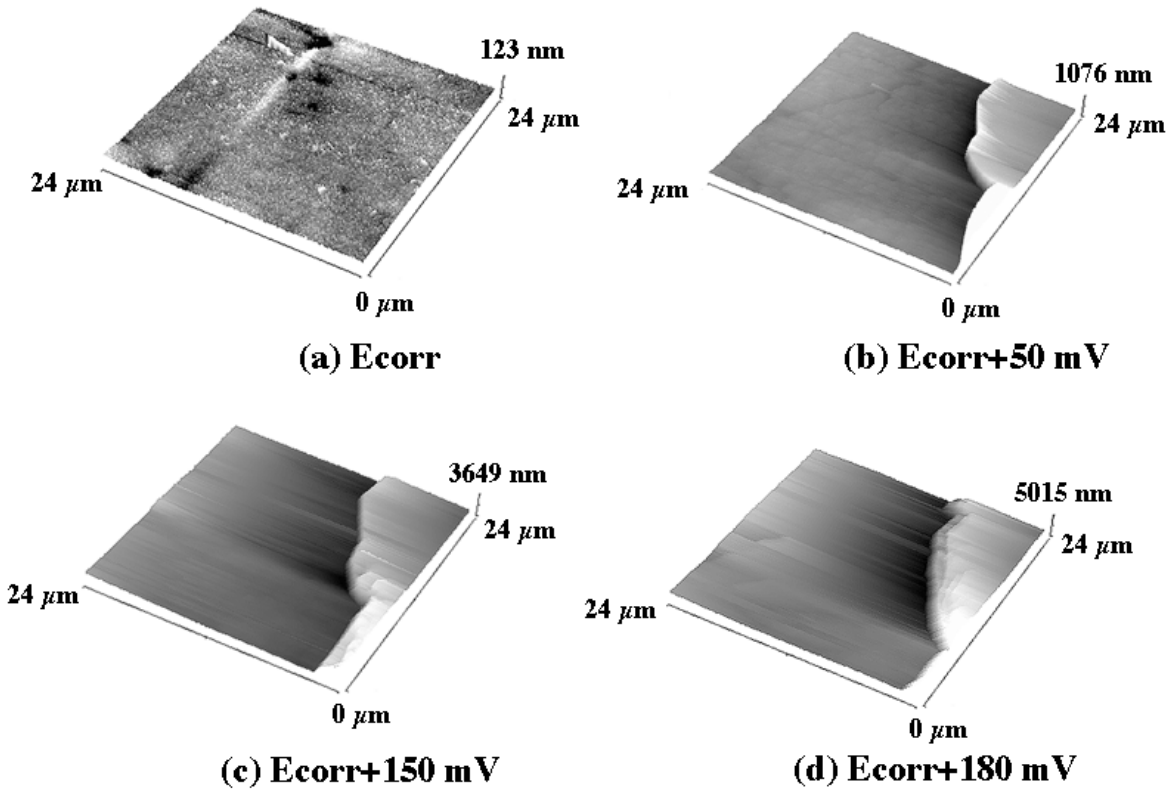

Figure 4. *In situ* EC-STM images of 2205 in 4M H_2S0_4 + 1M HCl.

On the other hand, the local dissolution behavior exhibited by UNS S32750 (Figure 5) was much more uniform than that of 2205. After the stabilization time at E_{corr}, some valley-like features could be observed, probably due to dissolution of inclusions or to the grinding process (Figure 5a). Dissolution processes were observed at low anodic potentials (E_{corr} + 60mV), although in this case no phases, only grain-like features, were distinguishable (Figure 5b). At higher potentials, but still in the active region, dissolution continued and the z-scale increased, reaching a maximum of approximately 1 μm (Figure 5c-d). The features on the surface were quite shallow and no sharp edges were observed as in the case of 2205.

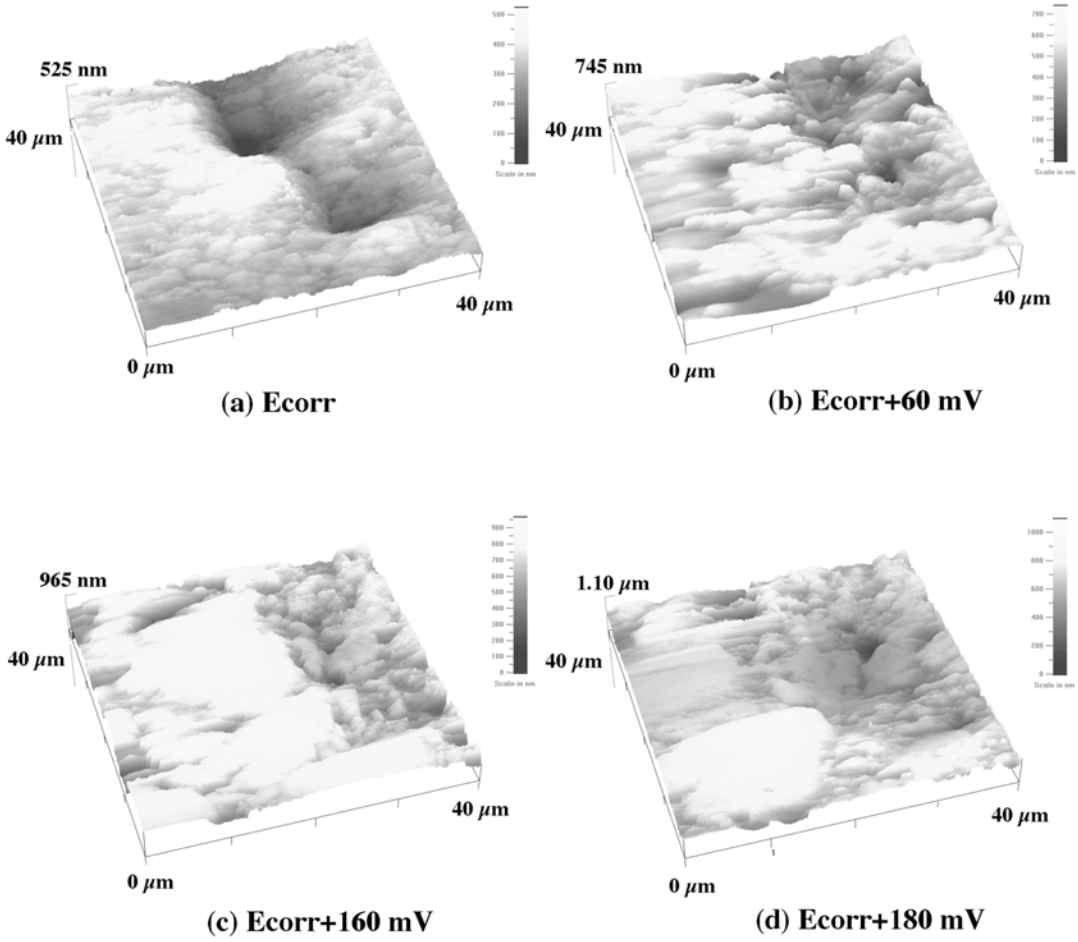

Figure 5. *In situ* EC-STM images of UNS S32750 in 4M H_2S0_4 + 1M HCl.

3.1.2 UNS S32304, UNS S31803, and UNS S32750 in 1M H_2S0_4 + 1M NaCl

The local dissolution behavior of UNS S32304, UNS S31803, UNS S32750 in 1M H_2S0_4 + 1M NaCl was studied in Ref. 84. The polarization curve of each steel showed a clear active current peak at low anodic potentials, and a passive region at higher potentials. In this case, the polarization curves of the steels did reflect the variation in the content of alloying elements (Figure 3, Ref. 84). As the content of alloying elements increased in the steel, the E_{corr} shifted to more noble potentials, and the critical and passive current densities decreased, indicating a significant increase in corrosion resistance.

The three steels exhibited also a different dissolution behavior at the local scale, and the EC-STM experiments provided additional information about how the dissolution processes actually took place. During the EC-STM measurements, the UNS S32304 samples exhibited pitting-like dissolution from potentials as low as E_{corr} + 110 mV, still in the active region. This phenomenon was not seen in the potentiodynamic measurements, probably because of the shorter measurement times, whereby pitting-like dissolution would not have time to develop.

Figure 6 shows a series of *in situ* images of UNS S32304 at increasing anodic potentials in the active range. In order to let E_{corr} stabilize, the sample was immersed during one hour in the solution, after which selective dissolution of the ferrite phase could be clearly seen. At E_{corr} + 10 mV, the dissolution of a non-metallic inclusion yielded a cavity, and re-deposited dissolution products could be distinguished on its left edge (Figure 6a). The cavity remained stable until E_{corr} + 110 mV (Figure 6b), when it began growing both laterally and in depth (Figure 6c-d). At E_{corr} + 320 mV the cavity drastically expanded, and at higher potentials the surface roughened considerably due to the nucleation and growth of pits (Figure 6e-f). Once the measurement was terminated, the surface appeared heavily corroded, being impossible to identify the phases through *ex situ* characterization. This was probably because the sample remained polarized at high potentials for a few hours, which enabled the nucleation and growth of numerous pits over almost the whole surface.

In another experiment series, a quite different local behavior of UNS S32304 was recorded. After immersion for one hour at E_{corr}, it was possible to distinguish the two phases due to the selective dissolution of ferrite (Figure 7a). For some unknown reason, the images in this series drifted from the starting area, i.e. not exactly the same area was imaged during the whole experiment, although some features were recognizable in all the images. At low anodic potentials, up to E_{corr} + 90 mV, the ferrite phase seemed to be dissolving at a slightly higher rate than austenite, which remained virtually unchanged.

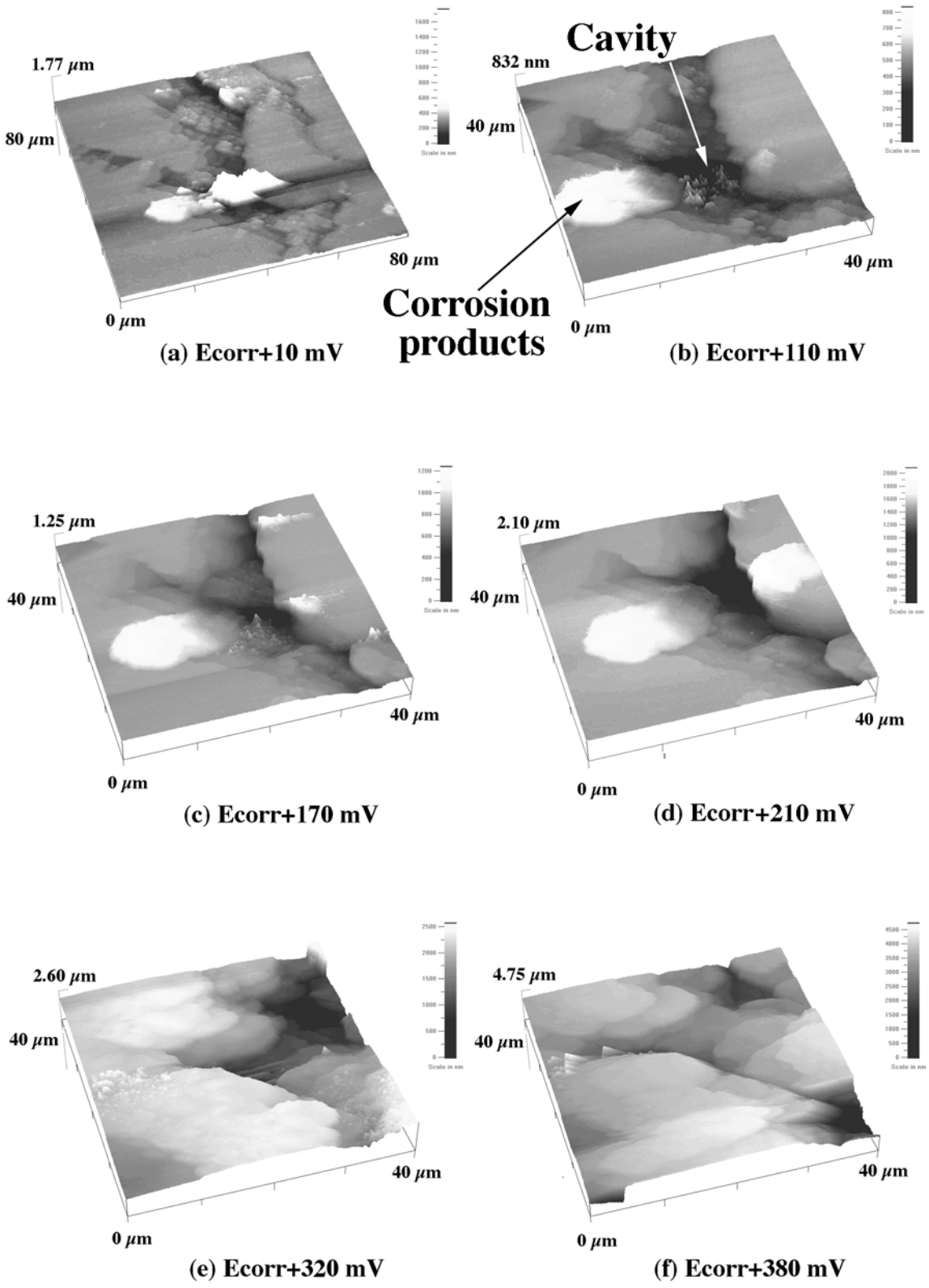

Figure 6. *In situ* STM images of UNS S32304 in 1M H_2SO_4 + 1M NaCl.

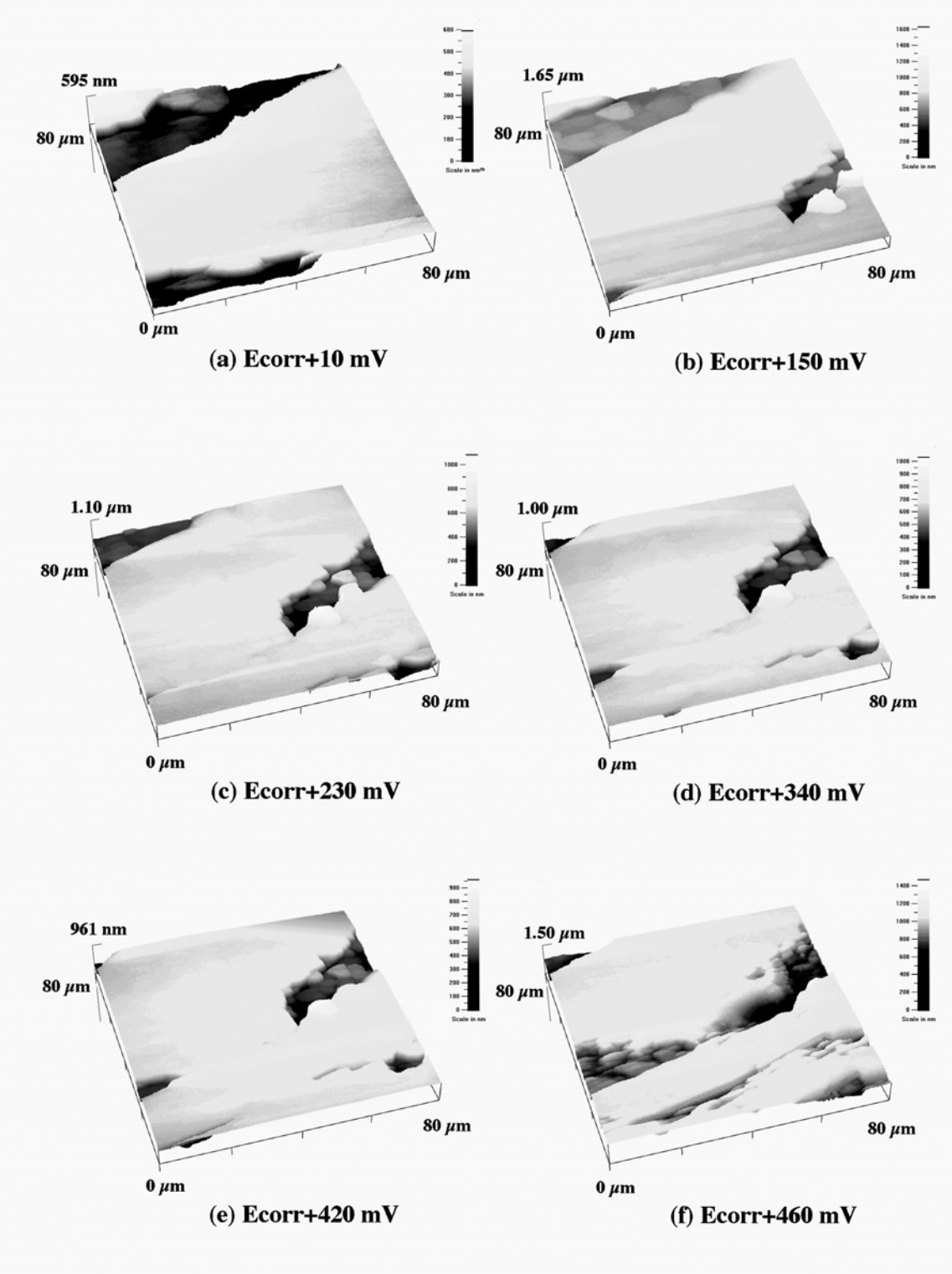

Figure 7. *In situ* STM images of UNS S32304 in 1M H_2SO_4 + 1M NaCl.

Due to the shift of the imaged area, a pit-like cavity, probably originating from dissolution from a non-metallic inclusion, appeared on the right side of the image (Figure 7b). In this case, however, the cavity did not grow in depth or laterally during the whole experiment. At higher anodic potentials, up to E_{corr} + 420 mV, the z-scale difference

decreased slightly, suggesting that in this potential range austenite was dissolving at a somewhat higher rate than ferrite (Figure 7b-e). At E_{corr} + 460 mV, the topography of the surface experienced a sudden modification, which may have been related to the active-passive transition (Figure 7f). Subsequent *ex situ* examination revealed selective dissolution of ferrite and of the phase boundaries, as well as significant pitting-like attacks at other locations over the surface.

In the same solution, UNS S31803 exhibited no significant ferrite selective dissolution at E_{corr}, and grinding marks could be discerned on the surface of the sample (Figure 8a). At low anodic potentials, ferrite selectively dissolved and the two phases could be easily distinguished (Figure 8b). At E_{corr} + 90 mV, austenite started to dissolve and the grinding marks became progressively blurred, while dune-shaped heaps started to appear along the phase boundaries (Figure 8c-f), probably originating from re-deposited dissolution products. Subsequent *ex situ* examination revealed no heap-like features on the surface, which could have been washed away when rinsing the sample. The step between austenite and ferrite decreased with time at higher anodic potentials, suggesting that austenite dissolved faster than ferrite in this potential range.

Comparing the results of UNS S32304 with those obtained in Ref. 82 for the coarse-grained 2205, it is possible to see that both steels exhibited the same selective dissolution pattern, indicating that the grain size does not play a major role in the dissolution behavior of DSS. The only significant difference between the two experiments was the z-scale between the phases, most likely due to the different aggressiveness of the solutions tested.

In spite of showing a clear peak in the active region of the potentiodynamic curve, the UNS S32750 showed a high degree of dissolution resistance in the 1M H_2SO_4 + 1M NaCl solution with EC-STM images that revealed no visible local dissolution in the active or passive potential regions (Figure 9, Ref. 84). Only randomly distributed ellipse-shaped features, with a z-scale not higher than 60 nm, were observed during the measurements. However, at very high potentials (E_{corr} + 1260 mV), the phases could be distinguished, together with evident grain boundary dissolution, suggesting transpassive dissolution as a possible cause for this phenomenon.[69]

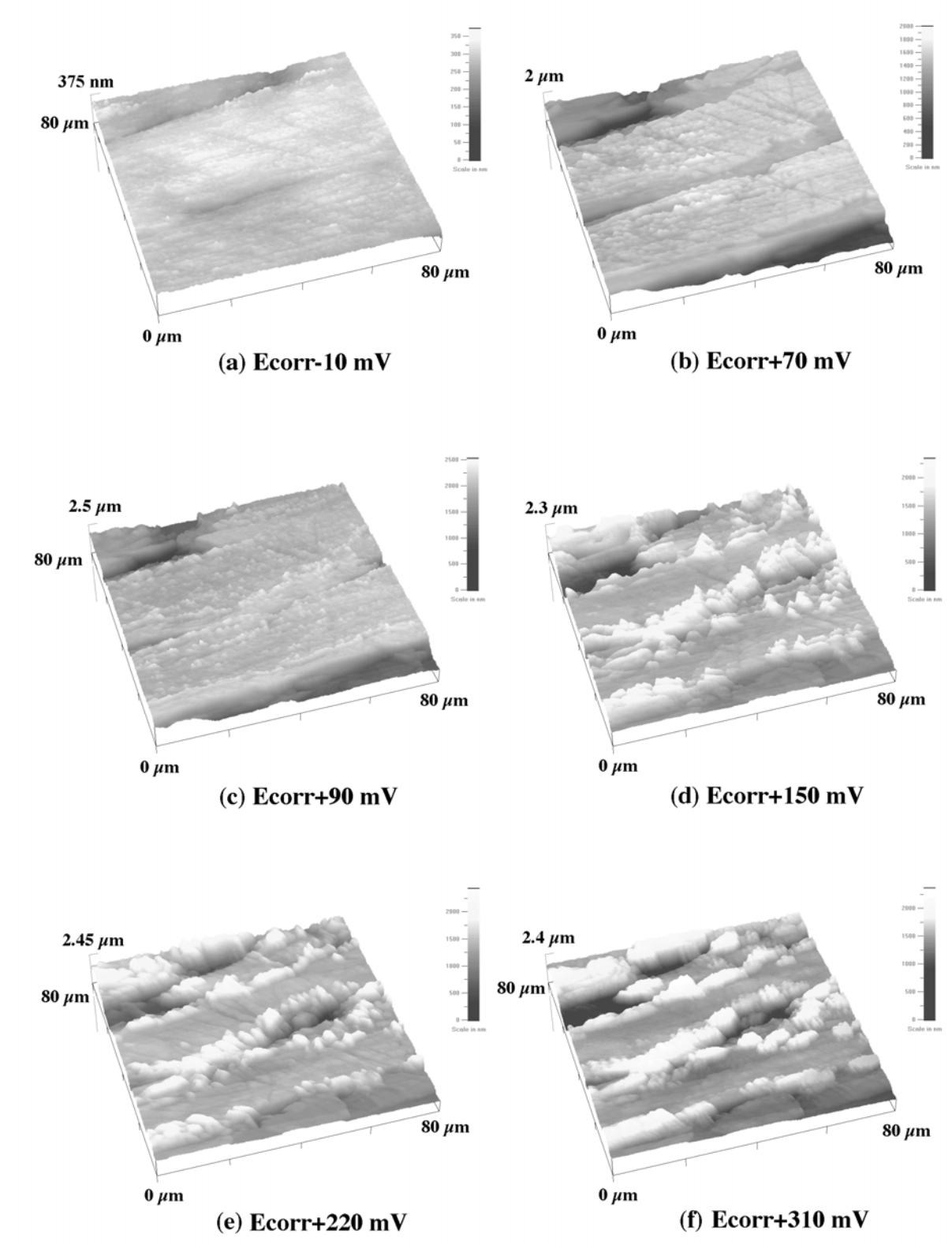

Figure 8. *In situ* STM images of UNS S31803 in 1M H_2SO_4 + 1M NaCl.

3.2 Scanning Kelvin Probe Force Microscopy

The results presented in this work are, to our best knowledge, the first application of SKPFM to the study of DSS. The goal of these experiments was to establish if there was a measurable Volta potential difference between ferrite and austenite that could give direct evidence of galvanic interactions between the two phases. In order to accomplish this, it was necessary to know the distribution of the phases, so that the Volta potential features in the SKPFM images could then be correlated to the microstructure of the steel. However, the traditional method used for the identification and characterization of the ferritic and austenitic phases in DSSs, surface etching, did not seem adequate in this case because it would have modified the surface oxide layer, and thereby the measured Volta potential. Thus, MFM appeared as the optimal technique to use because without the need for surface etching, it was capable of rendering a map of the phase distribution with sub-micron resolution. In addition, it was very easy to combine MFM with SKPFM by just changing some software parameters.

In general, the MFM images of DSSs are easy to interpret, although in some cases the magnetic domains of the ferrite phase can exhibit such different appearances, that the identification of the phases may become difficult. Therefore, some aspects should be taken into account in order to avoid misinterpretation of the images. One of the most important factors in MFM imaging is the actual orientation of the magnetic domains of the sample, which, in turn, depends on the crystallographic orientation of the ferrite. Therefore, it should be expected that ferrite grains with different crystallographic orientations yield different magnetic patterns in the MFM images. Other factors that can affect the contrast in the MFM images are the geometry of the magnetic domains, and the fact that even domains that are underneath the surface (i. e. non-superficial) can be detected, which may render different contrast than the superficial ones.

3.2.1 Non-exposed UNS S32304, UNS S31803, and UNS S32750.

The combination of MFM and SKPFM revealed a clear correlation between the Volta potential variation and the phase distribution in DSSs. The dominating feature in the SKPFM images obtained during the course of this work was that the ferrite phase corresponded to lower Volta potential regions, while austenite was associated to areas with

more noble potential. Figure 9 gives an example of the information that the combination of different SPM techniques can supply when applied to the investigation of DSS.

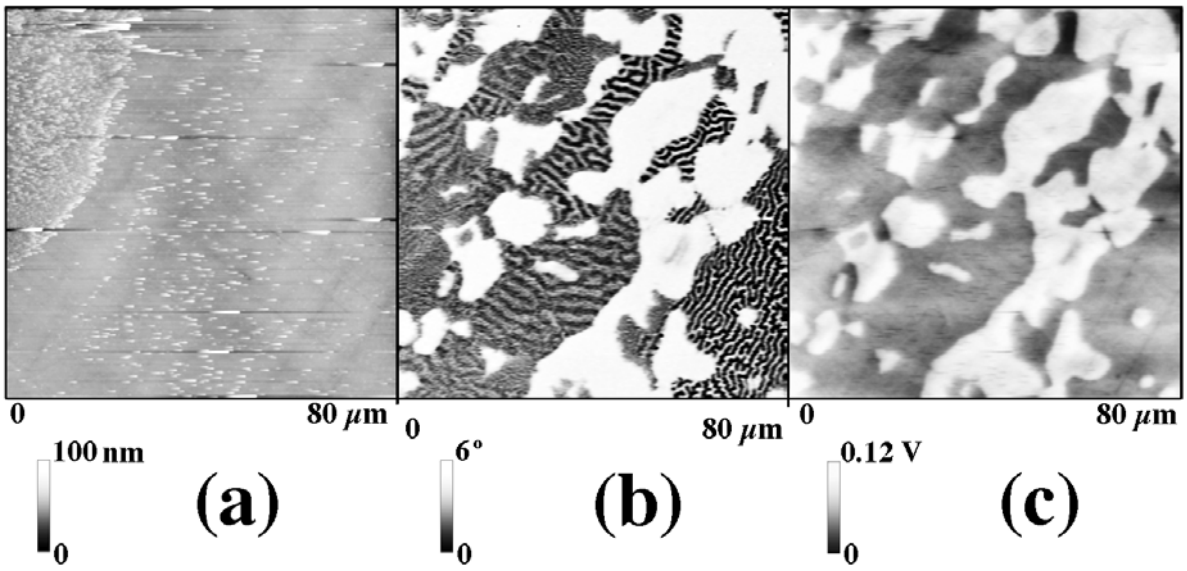

Figure 9. Polished UNS S32750 sample, scanned area 80 x 80 µm. (a) AFM surface topography (b) Magnetic domain distribution, (c) Volta potential distribution.

The topographic image of UNS S32750 (Figure 9a) showed a very flat surface where the only distinguishable features were some contamination particles and a few grinding scratches. From this image, it was not possible to distinguish the distribution of the ferritic and austenitic phases over the surface. On the other hand, the magnetic domain distribution presented in (Figure 9b) could easily be associated with the microstructure of the steel. The MFM technique was capable of clearly imaging the magnetic domain structure of the ferrite phase that surrounds the "islands" of austenite, appearing flat and uniform due to their paramagnetic properties. The correlation between the Volta potential variation (Figure 9c) and the phase distribution in the UNS S32750 sample (Figure 9b) was so clear, that the SKPFM image could almost be taken for a microstructure image of the surface. The highest Volta potential difference between the phases measured was approximately 80mV, but the recorded potential within the phases was far from uniform, with variations of up to 40 mV within both austenite and ferrite.

The other two steels studied, UNS S32304 and UNS S31803, exhibited the same type of features as UNS S32750. The only remarkable difference was that the ferrite phase near the

boundary to austenite for these two steels often displayed a lower Volta potential than the bulk ferrite. This could imply that these regions were more prone to local dissolution.

In the case of UNS S32304, the AFM image (Figure 10a) also presented a very smooth surface with some grinding scratches and small contamination particles, while the MFM image showed the phase distribution in this steel (Figure 10b).

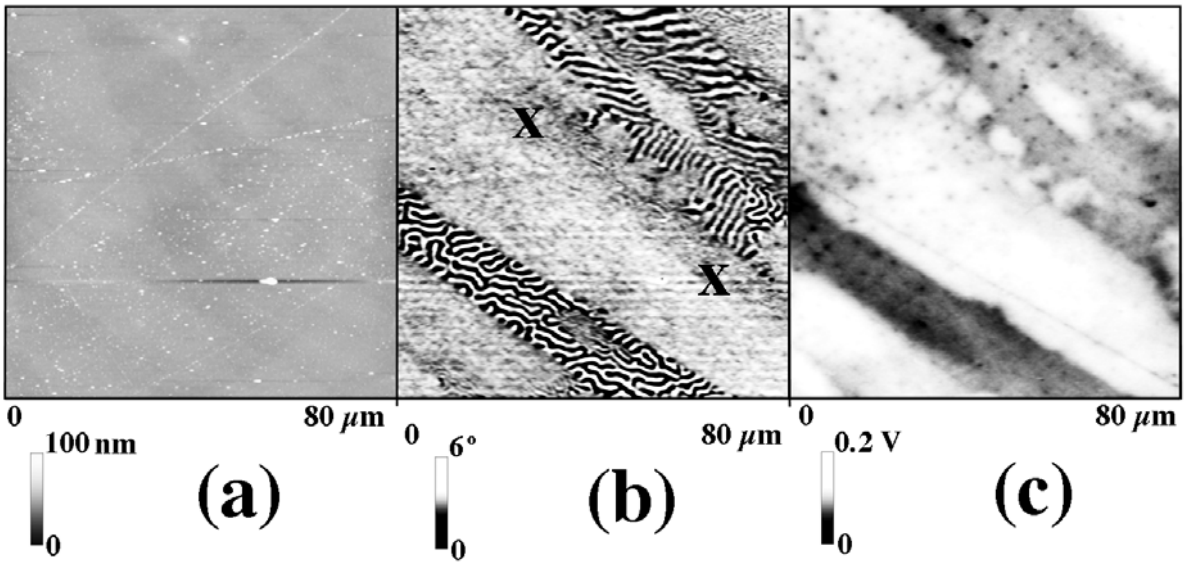

Figure 10. Polished UNS S32304 sample, scanned area 80 x 80 μm. (a) AFM surface topography b) Magnetic domain distribution, c) Volta potential distribution. X designates ferrite regions that did not exhibit the typical striped domain structure.

Clear bands of ferrite could be easily distinguished, but a closer look revealed other regions of ferrite (marked with X) that did not exhibit the more typical striped magnetic domain configuration, similar to the ferrite regions on the left part of Figure 9b. In this steel, the Volta potential distribution (Figure 10c) was also highly correlated to the phase distribution, with ferrite displaying lower Volta potential than austenite. The maximum Volta potential differences recorded were very similar to those of UNS S32750, approximately 80 mV between the phases and around 40 mV within the ferrite, but somewhat lower within the austenite (25 mV). In Figure 10c, several lines that remind of grinding scratches could be noticed, but it was remarkable that not all of these lines could be seen in the topographic image (Figure 10a). This could indicate that they were caused by defects on the surface due to the grinding process.

In the case of the polished UNS S31803 sample, it was also possible to identify the two phases, but in this case the correlation was not as straightforward as for the other two steels (Figure 11b).

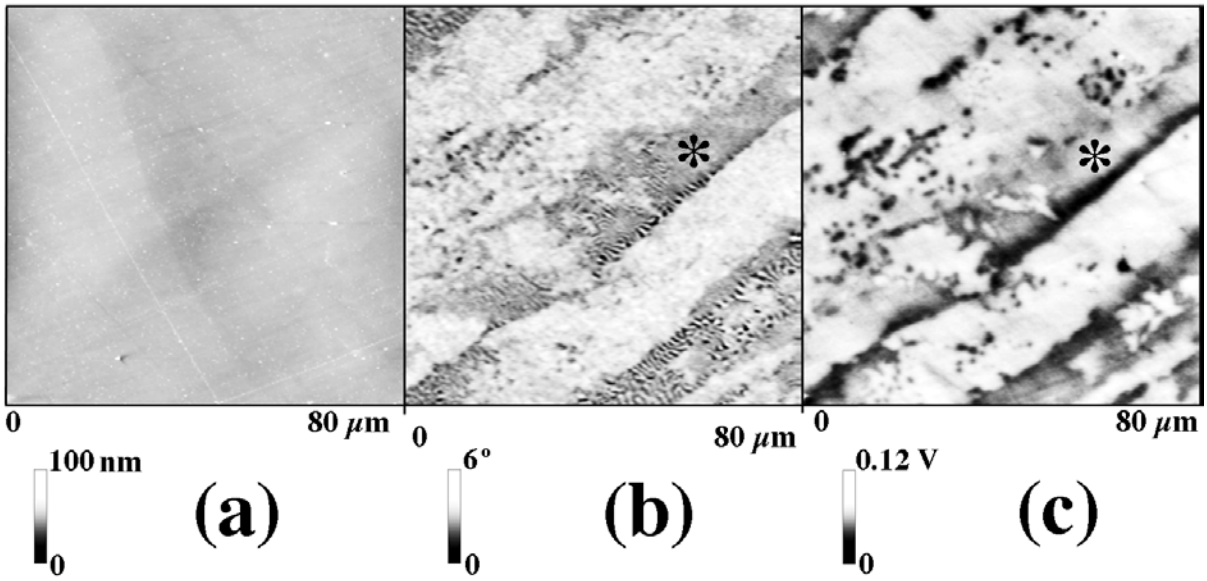

Figure 11. Polished UNS S31803 sample, scanned area 80 x 80 µm. (a) AFM surface topography (b) Magnetic domain distribution, (c) Volta potential distribution. * marks the region identified as ferrite in (b) that showed a Volta potential similar to austenite in (c).

The general correlation ferrite-low potential and austenite-high potential was maintained in the SKPFM image (Figure 11c), but the maximum Volta potential differences recorded were slightly lower than for the other two steels (approximately 50 mV between the phases). Within the phases, the variation could be just as high, which implied that in some places the potential of the austenite was indistinguishable from that of the ferrite (marked with * in Figure 11c). A possible explanation for this lack of correlation could be that the ferrite domains imaged by the MFM might actually have been non-superficial, so that the Volta potential measured would in fact correspond to the austenite phase.

3.2.2 Exposed UNS S32304 and UNS S32750.

Some measurements were also performed on samples that had been exposed during 30 minutes to a 1 M H_2SO_4 + 1 M NaCl solution at E_{corr}. The high-alloyed sample, UNS S32750, showed no noticeable differences with respect to the non-exposed condition.

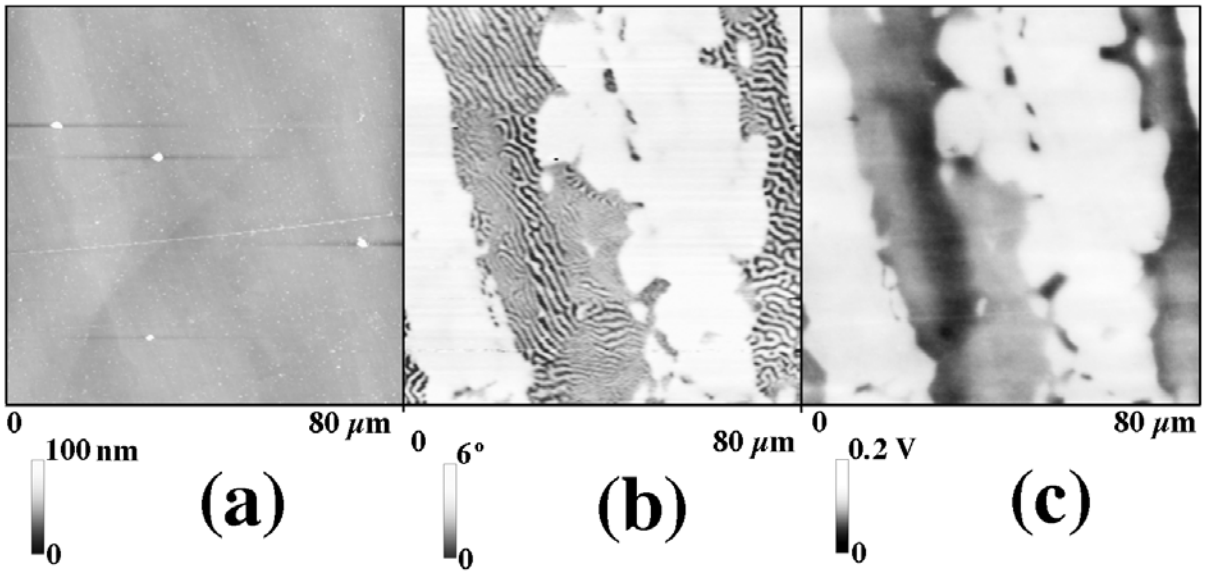

Figure 12. Exposed UNS S32750 sample, scanned area 80 x 80 µm. (a) AFM surface topography (b) Magnetic domain distribution, (c) Volta potential distribution.

From the topography image (Figure 12a), it was possible to see that the exposure to solution caused no measurable corrosion attack on this steel. The surface appeared very flat, showing only a few contamination particles and some grinding scratches. The MFM image (Figure 12b) distinctly brought out the phase distribution in the steel, which showed an excellent correlation to the Volta potential variation displayed in Figure 12c. As in the non-exposed sample, the ferrite phase corresponded to the low potential regions, and the austenite to more noble potential regions. The highest potential difference measured between the two phases was about 80 mV, and the variation within the ferrite was up to 40 mV, both values very similar to the non-exposed sample. The austenite, however, presented a somewhat more uniform potential, with the highest variation being around 25 mV.

On the contrary, the exposed sample of UNS S32304 presented a great deal of differences compared to the non-exposed sample. The topography image showed, as expected, evident signs of corrosion (Figure 13a), with a z-height scale significantly higher than that of the non-exposed sample. It was more difficult to distinguish the phase distribution from the MFM image in this case than for the non-exposed sample (Figure 13b).

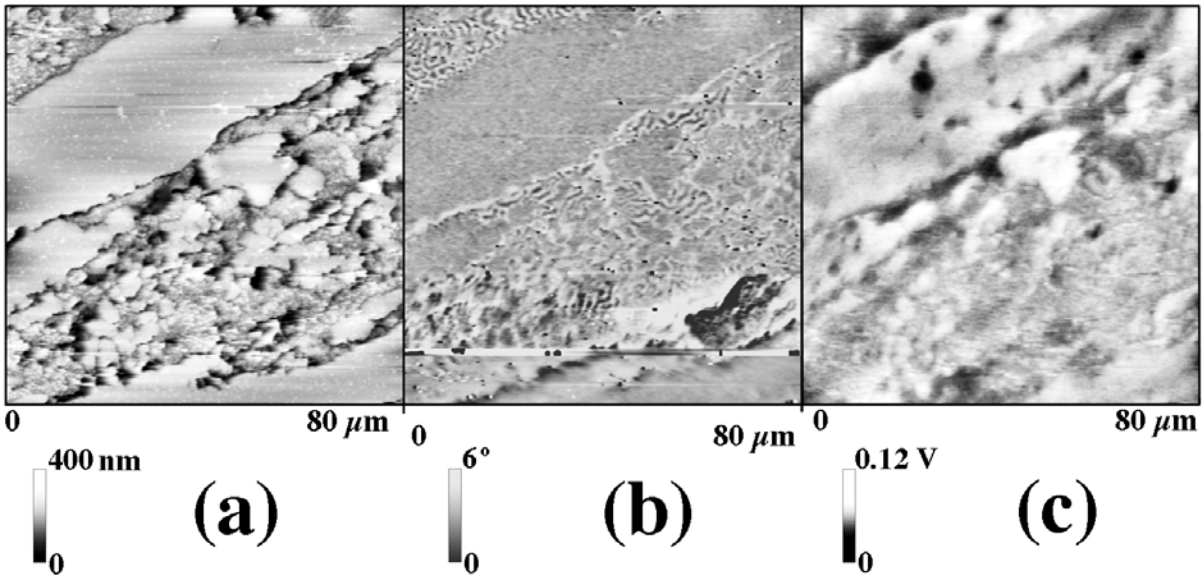

Figure 13. Exposed UNS S32304 sample, scanned area 80 x 80 µm. (a) AFM surface topography (b) Magnetic domain distribution, (c) Volta potential distribution.

Despite this, some magnetic domains could still be discerned, making possible a rough identification of the phases. Comparing the AFM and MFM images, it was possible to state that the ferrite phase had been selectively dissolved, which was in accordance with earlier EC-STM observations. The Volta potential variation (Figure 13c) showed a weaker correlation with the phase distribution than the non-exposed sample. Still, most of the non-corroded parts that were associated with austenite presented a higher Volta potential than the regions identified as ferrite. It was remarkable that the Volta potential variation, with a maximum recorded potential difference of approximately 40 mV over the whole surface, was significantly more uniform than for the non-corroded sample.

3.3 Scanning Auger Electron Spectroscopy

In the literature, a few studies have been reported using Auger Electron Spectroscopy (AES) to study the chemical composition of the passive film of DSSs.[14, 70] These studies, however, included no information related to the phase boundary region. Therefore, it seemed interesting to investigate the elemental distribution through the austenite-ferrite interface with a high-resolution technique in order to see if it differed from that of the bulk phases. In this way, it could be possible to elucidate if there was depletion of certain alloying elements at the

phase boundary region that could account for the EC-STM observations that the ferrite near the phase boundary tends to dissolve at a faster rate than bulk ferrite. Moreover, it seemed relevant to perform the SAES line-profiles on the alloy surface layer at the oxide/metal interface, where N and Ni have been reported to show enrichment compared to the bulk concentration. [14, 70] In this way, more knowledge could be gained about this layer, which seems to be of key importance for the corrosion properties of stainless steels.

As can be seen from Figure 14, Figure 15, and Figure 16, the line-profiles for the three DSSs presented, qualitatively, the same type of general features. The ferrite stabilizers, Cr and Mo, were partitioned to the ferrite phase, while the austenite stabilizers, Ni and N, were partitioned to the austenite. The transition at the phase boundary was quite smooth for all the elements investigated in all the steels, and no visible depletion or enrichment of any element could be distinguished. The mean values obtained of each element on the ferrite and austenite were averaged, and the resulting value was compared to the bulk concentration, which confirmed the enrichment of Ni at the alloy surface layer on both austenite and ferrite, and of N on the austenite.

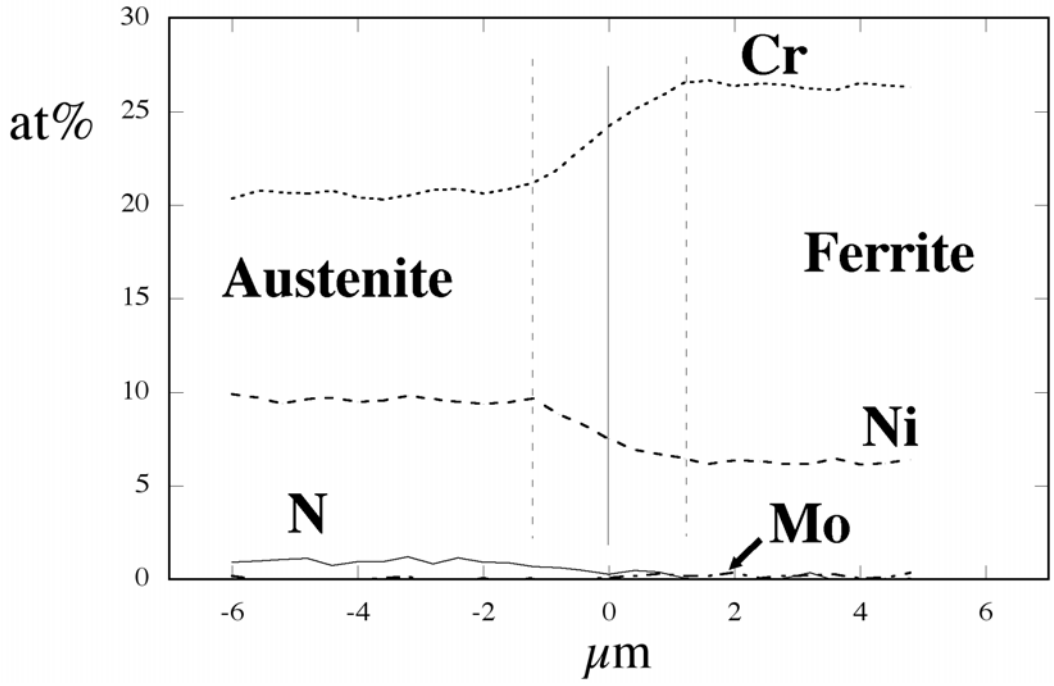

Figure 14. SAES line-profile over the phase boundary region, on the alloy surface layer at the oxide/metal interface for UNS S32304.

Comparing the line-profiles of the different DSSs, it could be seen that Cr and Mo were more partitioned, i.e. there was a larger difference in concentration between the phases, in the lower alloyed steels. The line-profiles of UNS S31803 and UNS S32750 could be

compared to the concentration values obtained at the alloy surface layers by other researchers.[14, 70] The profile for UNS S32750 agreed quite well with the reported values, however, the profile for UNS S31803 showed consistently higher Cr and lower Ni concentration values than those reported in literature. Insufficient sputtering of the passive film was the suggested explanation for this observation because of the expected Cr-enrichment and Ni-depletion in the passive film.

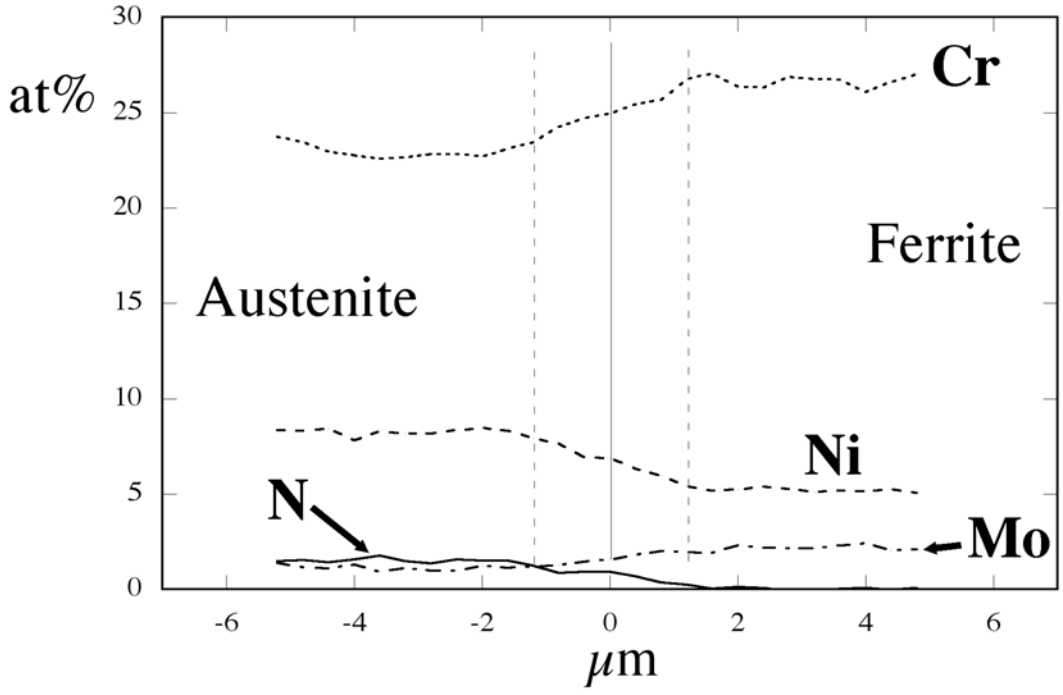

Figure 15. SAES line-profile over the phase boundary region, on the alloy surface layer at the oxide/metal interface for UNS S31803.

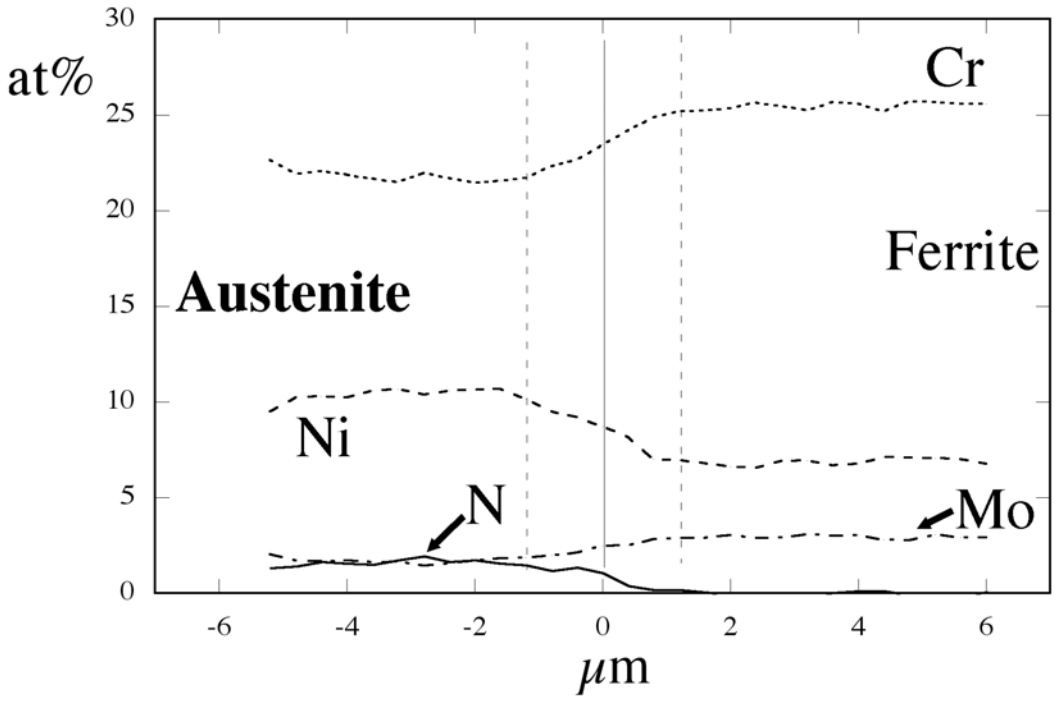

Figure 16. SAES line-profile over the phase boundary region, on the alloy surface layer at the oxide/metal interface for UNS S32750.

3.4 Scanning Electrochemical Microscopy

In the course of these studies, a great deal of effort was dedicated to the SECM technique. Unfortunately, due to considerable experimental difficulties, it was not possible to obtain relevant results with this technique despite the same instrument had been successfully used for the EC-STM measurements. In the SECM measurements, three factors significantly increased the experimental difficulty compared to EC-STM: the need for optimal insulation of the tip, the lack of feedback circuit, and the requirement of a background noise in the pA range.

In order to detect the faradaic current from the corrosion processes occurring at the surface, the tip needed a more accurate insulation than for the EC-STM measurements. Although this caused a certain amount of extra-work, it was relatively easy to obtain an optimal tip insulation. The lack of feedback circuit required the surface of the sample to be almost completely horizontal, which meant a very flat surface with very low tilt. With a polishing-aid, a tilt-stage and a great deal of practice, it was possible to obtain extremely flat surfaces, with a tilt lower than 1 nm per μm. However, the background noise proved to be too difficult to control. The noise level was in the nA range, and only in a couple of isolated

occasions it was possible to discern some electrochemical signal, probably originating from the corrosion processes taking place on the surface.

The SECM experiments were interrupted due to lack of time, but it was felt that once the cause of the high background noise was found and controlled, it should finally be possible to use this technique to its full capacity.

4. DISCUSSION

4.1 Local vs. Global Experiments

Corrosion science is a discipline that is spread over a broad range of length scales that are often closely related. For example, the corrosion resistance of engineering materials (macroscopic) is strongly dependent on their microstructural properties (microscopic). Therefore, it seems evident that the macroscopic corrosion behavior of engineering materials will be better understood if the underlying chemical, physical and electrochemical phenomena involved can be investigated on a micrometer or nanometer scale. Thus, it is easy to see that parallel microscopic and macroscopic investigations are necessary in order to gain deeper understanding about the corrosion behavior of engineering materials.[71] The recent development in the field of local probing techniques has opened the microscopic frontier for corrosion investigations, providing a great quantity of new information about the corrosion processes at a local scale. The interconnection of the microscopic and macroscopic scales will be of utmost importance in future investigations of complex technological systems,[9] although unfortunately, very few studies have been reported that emphasize the relation between effects measured at different scales.[71]

All this is especially relevant in the case of DSS, where the corrosion behavior of the individual phases is a key factor for understanding the corrosion properties of the whole material. During the course of this work (Refs. 82-84), conventional electrochemical techniques were used in combination with EC-STM in an attempt to gain further insight into the corrosion behavior of DSS in acidic-chloride solutions. In this work, the main difficulty in correlating the local and global information was mainly due to the difference in time and length scales, and from the inherently different type of data obtained from each technique.

The conventional electrochemical techniques employed during the course of these studies gave information about the electrochemical activity of the sample in the form of current density. EC-STM, on the other hand, showed the evolution of the surface topography of the electrode. Thus, the parameters to be correlated were current density over a large surface area and topography changes over a small area which, although lacking a direct comparison, still could be connected to each other.

The difference in time scale of the experiments added further complication to the interconnection of results. Potentiodynamic polarization curves were obtained over a period of the order of one hour, whereas EC-STM experiments could last over 10 hours in order to cover the same potential range. This inherent difference in time scale turned out to be of special relevance in processes where induction time was an important factor, such as in the pitting-like dissolution observed on UNS S32304 in Ref. 84. In this case, fast potentiodynamic scans seemed not to allow sufficient time for the growth of pits, whereas during the long potentiostatic polarization measurements in the EC-STM measurements, pits had time to grow and heavily corrode the sample.

The conventional electrochemical techniques used in this work measured surfaces of ~1 cm^2, therefore yielding only global information about the corrosion behavior of the sample. On the other hand, the EC-STM system probed surfaces of the order of ~10^{-5} to 10^{-4} cm^2, yielding localized information about the dissolution processes. Such small-scale measurements were needed for monitoring the local electrochemical behavior of the individual phases of DSS. This local information is of great value, but caution must be taken when extrapolating the local results to describe global processes occurring over the whole surface, because there is a risk of overestimating the importance of the imaged events. For example, when studying localized corrosion phenomena with EC-STM, repeated measurements of different single events may give quite different results, as seen for UNS S32304 in Ref. 84, making necessary a global picture of the corrosion behavior for their understanding.

Thus, the comparison between local and global experiments is not immediate, but the experimental differences can be overcome if the appropriate measures are taken. For instance, it is of supreme importance to repeat as many different local measurements as possible on the same material, so that it is possible to monitor the whole range of particularities and local events that can take place on the surface. Careful subsequent *ex situ* examination should be able to give an approximation to the general behavior of the sample as well as indicating the possible singularities present, such as non-metallic inclusions or precipitates. All this should

give solid grounds for successfully relating the global and local methods, which is of key importance, especially when studying highly heterogeneous materials, such as DSS.

In all, the new localized techniques in general, and EC-STM in particular, represent a powerful tool capable of producing images of events never directly observed before, which may lead to improved hypotheses of the underlying mechanisms behind them.[9] Moreover, in certain cases, these observations can even result in quantitative observations that can be useful in the development of mathematical models that can validate those hypotheses.[9] However, only when this local information is considered within the context of the global processes can the full potential of these techniques be attained.

4.2 Combination of Local Probing Techniques

In corrosion investigations, different techniques are often used in order to cover different aspects of the corrosion behavior of a sample in a certain solution. The information obtained by means of these techniques can be regarded as pieces of a jigsaw puzzle that, when put together, can lead to a deeper understanding of the investigated phenomena. Thus, the combination of these different techniques can become an important factor for gaining a more comprehensive understanding of the corrosion processes involved. Moreover, the combination of different techniques might be especially helpful when using a novel technique with insufficient amount of background data. Considering that the interpretation of the new results might not always be straightforward, their comparison with results from more established techniques or from literature might be necessary for their understanding.

During the course of these studies, several high-resolution techniques with comparable lateral resolution (~ 1μm) have been used in order to investigate the corrosion behavior of DSS in acidic-chloride solutions. The EC-STM results presented in this study show how localized *in situ* techniques can contribute to the elucidation of corrosion mechanisms on a local scale, by permitting single events to be monitored while on-going. By means of EC-STM, it was possible to follow in detail processes such as the growth of a single pit (Ref. 84) or the selective dissolution of a single phase in a DSS (Refs. 82 and 84). On the other hand, SKPFM was used in Ref. 85 to measure the Volta potential variation over the surface of DSS with the aim of correlating it to the phase distribution visualized by MFM. In this way, a significant Volta potential difference between ferrite and austenite was measured. In Ref. 86, SAES was used for studying the chemical composition across the phase boundary

at the alloy surface layer. The concentration line-profiles obtained showed the partitioning of the alloying elements between the two phases, as well as the enrichment of N and Ni at the alloy surface layer.

The fact that all these techniques possess the same range of lateral resolution facilitates their combination and makes possible a direct comparison between them. The most obvious example of the advantages of combining different techniques is probably Ref. 85, where the combination of the topographic, magnetic and potential data was done directly with the same instrument, resulting in very important information. But as a matter of fact, the comparison of results can be extended also to other techniques rather directly. For example, in Ref. 85, UNS S32304 was investigated before and after exposure to a 1 M H_2SO_4 + 1 M NaCl solution at E_{corr} for 30 minutes. The AFM-topography image of the exposed sample showed that one of the phases had selectively corroded during exposure. The MFM image identified this phase as ferrite, which showed a lower Volta potential in the SKPFM image. These measurements not only confirmed the behavior monitored *in situ* by EC-STM, but also gave a direct account for the possibility of galvanic interaction between phases that had been suggested in Ref. 84. The galvanic interaction between the phases had been previously reported by Symniotis[72-74] who had measured it indirectly with conventional electrochemical techniques. Hence, an excellent example of the importance of complementing the global investigations with localized studies.

The comparison of results obtained by means of different techniques can easily be extended to other local probing methods, as long as the results are compatible. For instance, Perren *et al.*[18] used a microelectrochemical method that made possible the measurement of individual potentiodynamic polarization curves of the single phases of DSS. Their results showed that when the two phases of a DSS had similar PRE values, their individual polarization curves presented the same type of features, which would be an indication of overall uniform corrosion behavior. However, measurements at the phase boundary region showed how the galvanic interactions between phases might alter this uniform behavior. These results can be compared to those obtained through the course of this work because they monitor the same type of phenomena, and they do it on the same length scale. The chemical composition information obtained by SAES in Ref. 86 showed that UNS S32750 had the smallest composition difference between the phases. This was reflected in the EC-STM measurements, where this steel showed a quite uniform dissolution behavior, with no evidence of selective dissolution (Ref. 83). Although no indications of galvanic interactions were monitored by EC-STM for this steel, significant Volta potential differences between

ferrite and austenite were measured by SKPFM, both before and after exposure to solution (Ref. 85). This might seem contradictory at a first glance, but it has to be taken into account that although the Volta potential is a measure of the driving force for galvanic corrosion, it is not capable of giving quantitative kinetic information about corrosion rates. Thus, even if there is a Volta potential difference between the phases, galvanic interactions like those reported by Perren *et al.* can only take place if all the necessary conditions are fulfilled.

Thus, the combination of the different local probing techniques used in this work and their comparison to other techniques of similar lateral resolution found in literature have been proven to be extremely useful. Each technique has made its little contribution and helped rendering this immense jigsaw puzzle of the corrosion behavior of DSS a bit more intelligible. Due to experimental difficulties encountered, the only regret has been the unsuccessful attempts to perform SECM measurements on the same system. It is clear that the information yielded by this technique, electrochemical current distribution over the surface of the sample with sub-micron resolution, would have been of great value, and easily comparable to the other techniques used in these studies.

4.3 Influence of the Alloying Elements

The use of DSSs with different alloying contents in these studies has made possible a comparison of their dissolution behavior in acidic-chloride solutions in terms of their alloying elements. However, the variation of alloying elements in these DSSs is not systematic, which makes it difficult to attribute a certain modification in the corrosion behavior to a particular alloying element. Nevertheless, it is still possible to point towards certain tendencies in how the addition of certain alloying elements affects the corrosion behavior of the steels.

The principal differences regarding the alloying elements between the three types of DSSs investigated are due to differences in their alloying contents of Mo and N, and to a lesser extent, Cr and Ni (Table I). From this compositional difference, the steels are expected to show a varying degree of corrosion resistance as the alloying contents change. Although the results presented in this study indeed show such a tendency, the corrosion behavior of DSS is more complicated than just a cause-effect relationship between corrosion resistance and the content of alloying elements, because the partitioning of the alloying elements between the phases also plays an important role.

N affects the corrosion behavior of DSS in a twofold way. On the one hand it is in itself a beneficial element against corrosion, and on the other hand it reduces the partitioning of Cr and Mo between the phases by allowing a higher content of Cr and Mo in the austenite.[10, 13, 16-18, 75] Since N is almost insoluble in ferrite, practically all N is concentrated in the austenite. Therefore, it is easy to see that N improves mainly the corrosion resistance of the austenite phase. This is a way of leading towards DSSs of well-balanced composition, i.e. with phases of comparable corrosion resistance, which is of key importance since the corrosion resistance of DSS is governed by that of its weakest phase.[10-12, 16-18] The partition coefficients calculated from the SAES line-profiles (Table III, Ref. 86) corroborate this behavior, with UNS S32750, the highest alloyed DSS, showing the smallest difference in composition between phases.

Quantifying the corrosion resistance of stainless steel is a difficult task because there are many factors involved that must be taken into account. The PRE is an empirical expression that was developed for ranking the resistance of austenitic stainless steel against pitting corrosion in terms of its Cr, Mo and N contents. Due to its simplicity, the PRE value has found widespread application among corrosion scientists, even when pitting is not the main form of corrosion studied. This might not necessarily be wrong, as long as it is used with caution. For example, in the present studies the phenomenon studied has been active dissolution, but since Cr, Mo and N are known to depress active dissolution,[68] the PRE values may still be used qualitatively as a rough measure of resistance against active dissolution. In fact, an expression very similar to the PRE formula has been reported to correlate the active dissolution rates of DSS in acidic-chloride solutions to the Cr, Mo and N contents.[72]

Due to the partitioning of the alloying elements between the phases, it has been suggested that separate PRE values for DSS should be calculated for each phase. [10-12, 16-18] However, confusion may arise when choosing the factor for N to be used in the PRE formula, because the use of different values may lead to contradictory conclusions about which phase is more resistant in a certain DSS. Besides, no influences from other alloying elements or synergisms between them are taken into account by the PRE formula. Therefore, even if the application of the PRE to DSS is quite widespread, it must be done with great caution and bearing in mind all its limitations.

Of all the DSSs investigated, only UNS S32750 is manufactured to have equal PRE values for both phases, implying that the alloying elements are partitioned in such a way that both phases exhibit equal corrosion resistance. This seemed to be corroborated by the EC-STM measurements, where the phases of UNS S32750 exhibited a fairly uniform dissolution

behavior (Ref. 83). On the other hand, all the other DSSs investigated exhibited selective dissolution in the acidic-chloride solutions tested. In general, the dissolution behavior of these DSSs followed the same pattern; preferential dissolution of ferrite at low anodic potentials, and activation of austenite at higher anodic potentials in the active region. In the case of UNS S32304, ferrite dissolved selectively already at E_{corr}, probably due to the low Mo content of this steel. Since Mo partitions to ferrite, the addition of Mo affects this phase to a larger degree than austenite. Indeed, the increase to 3% of the Mo concentration in UNS S31803 seemed to significantly strengthen the ferrite phase of this steel, which was capable of resisting selective dissolution at E_{corr} even in very aggressive solutions (Ref. 82). But it is not only the ferrite phase that seemed stronger in UNS S31803 with respect to UNS S32304, the phase boundaries in general also seemed to be less selectively attacked. A possible explanation for this phenomenon might be found in the Mo-N interaction. Several theories have been proposed to explain the mechanism of this synergism,[76-80] but more knowledge is still needed to formulate a comprehensive theory. Clayton *et al.* proposed the possibility that Mo, Ni and N, enriched at the alloy surface layer adjacent to the passive film, could form a mixed nitride phase that would preferentially nucleate at high-energy sites.[76-78] The SAES measurements in Ref. 86 showed no enrichment of Mo at the alloy surface layer, suggesting that the Mo content would be too low to form a continuous nitride phase. However, if small clusters of this nitride phase would nucleate at weaker sites, such as phase boundaries, these would be considerably strengthened, which could account for the EC-STM observations of UNS S31803.

4.4 Influence of the Phase Boundary Regions

The singularity of the phase boundaries is a factor that must be seriously considered when studying DSS. Within a distance of a few micrometers, large variations in alloying element concentration and Volta potential arise, which may lead to a locally different dissolution behavior compared to the bulk phase region. Besides, the phase boundaries are preferential sites for the precipitation of secondary phases, which usually decreases the corrosion resistance of the steel by providing starting points for localized corrosion.[4-6, 10, 81] The small investigated surface area offered by the local techniques used in these studies makes it difficult to obtain representative observations. Nevertheless such a tendency was indeed observed. Non-metallic inclusions and elongated cavities in the phase boundary region

of UNS S32304 and UNS S31803 were imaged by EC-STM in Ref. 84. Subsequent *ex situ* examinations revealed that UNS S32304 showed a certain degree of phase boundary dissolution, while UNS S31803 exhibited significantly less. On the other hand, SKPFM measured lower Volta potential values at the phase boundary than in the bulk phase, suggesting stronger susceptibility to corrosion attacks.

During the EC-STM measurements, a remarkable phenomenon was repeatedly observed. In the course of selective dissolution, the ferrite phase nearest to the phase boundary seemed to dissolve at a higher rate than the bulk ferrite (Figure 17). This sort of behavior has also been reported by other authors,[45] but the reason behind is not clear. Local galvanic interactions or local depletion of alloying elements were proposed as possible causes in Ref. 82.

The SAES line-profiles from Ref. 86 showed no depletion of alloying elements in the phase boundary region. However, in order to be able to discard this possibility with more certainty, new SAES measurements with improved resolution should be performed. Moreover, these measurements should be carried out with a lower level of background noise, so that it is possible to obtain reliable readings of the N concentration.

On the other hand, the SKPFM measurements in Ref. 85 showed, for UNS S32304 and UNS S31803, that the Volta potential of the ferrite adjacent to the phase boundary was often lower than that of the bulk ferrite. In fact, the resemblance of the EC-STM and SKPFM profiles shown in Figure 17 is quite remarkable, suggesting that the phenomenon observed with EC-STM might be caused by local galvanic interactions at the phase boundary. It is noteworthy that the SKPFM profiles for UNS S32750 showed no such features, possibly because the phase boundaries in this steel might no longer be weaker points.

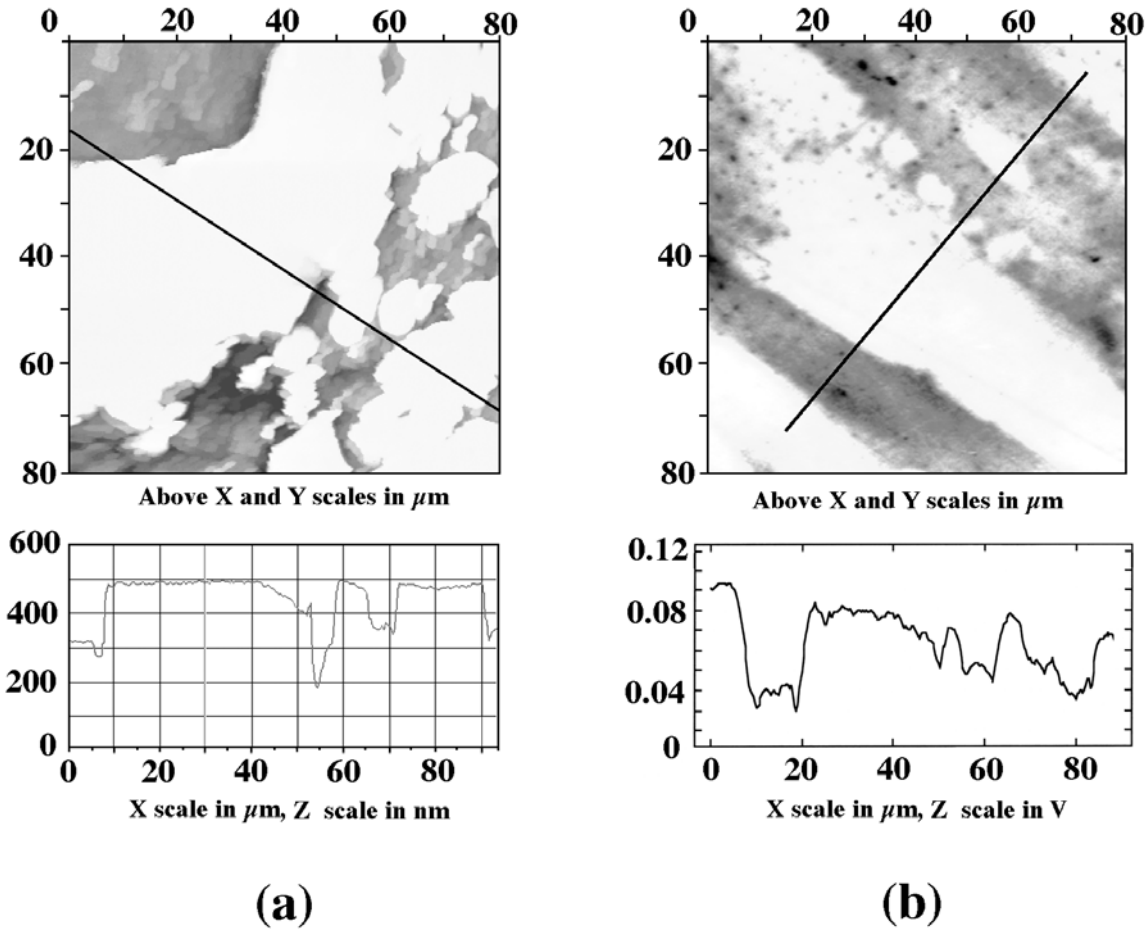

Figure 17. (a) STM height profile along the marked line, (b) Volta potential profile along the marked line.

5. CONCLUDING REMARKS

The results presented in this study clearly demonstrate the local nature of corrosion processes. Therefore, it is easy to realize the benefits of using high-resolution local probing techniques for corrosion science studies. Each technique has been used to investigate a different aspect of the corrosion behavior of DSS in acidic-chloride solutions, and the combination of the results has been an important factor for gaining a more comprehensive understanding of the processes involved. The most important techniques used within this work, together with the experienced capabilities, are summarized below:

- *In situ* EC-STM permits direct monitoring of electrochemical processes with sub-micron resolution, which, in the best case, only can be resolved indirectly by conventional

electrochemical techniques. Dissolution processes in commercial DSS can be followed in real time, thanks to the adequate lateral and time resolution offered by this technique.

- MFM is capable of imaging the phase distribution in DSS with sub-micron resolution, and without the need for the traditional surface etching.
- SKPFM measures the Volta potential distribution over the surface of DSS with sub-micron resolution. The Volta potential gives a measure of the relative nobility of the phases, and has been related to E_{corr}.
- SAES has shown that the composition gradient at the phase boundaries is narrower than 2 μm. New measurements with higher resolution and lower background noise would be desirable for a better characterization of the chemical composition across the phase boundary.
- SECM might provide extremely useful information about the local electrochemical processes occurring on the surface. Once the experimental difficulties have been overcome, it would be most interesting to apply SECM to the study of DSS.

The connection between macroscopic and microscopic information is extremely important, especially for localized processes like local dissolution or pitting corrosion. Parallel macroscopic experiments, combined with *ex situ* characterization will always be necessary in order to complement the information obtained with local techniques. In this way, a more comprehensive understanding of the processes involved can be gained.

The partitioning behavior of the alloying elements is of key importance for understanding the corrosion behavior of DSSs. The phases of higher alloyed steels exhibited smaller differences in corrosion resistance and in composition. Higher contents of Cr, Mo and N strengthened both phases as well as the phase boundaries. DSSs with phases having similar corrosion resistance showed a more uniform dissolution behavior.

In the literature, several theories have been proposed to explain the beneficial role of Mo and N for the corrosion resistance of stainless steels. The results presented in this study suggest that explanations of the synergism between Mo and N in DSS have to consider their influence on weaker sites, such as phase boundaries.

The Volta potential variation is strongly correlated to the phase distribution. The Volta potential difference between ferrite and austenite has been found to be measurable and significant. Ferrite is in general associated with lower Volta potential regions, and austenite to more noble potential regions.

Ferrite adjacent to the phase boundary showed lower Volta potential values than bulk ferrite, suggesting that the higher dissolution rate of this region in acidic-chloride solutions could be due to local galvanic interactions between the phases.

6. ACKNOWLEDGEMENTS

Thanks to Ulf Kivisäkk (AB Sandvik Steel), Dr. Lena Wegrelius, Tekn. Lic. Anna Iversen, and Elisabet Alfonsson (at Avesta Polarit AB) and Dr. Rachel Pettersson (Swedish Institute for Metals Research) for valuable comments and constructive criticism of my work. Ulf and Lena also are thanked for arranging all the practical details during my pleasant stays at Sandviken and Avesta.

AB Sandvik Steel, Avesta Sheffield AB, and the Brinell Centre at KTH are acknowledged for the financial support to this work.

7. REFERENCES

1. J. Beddoes and J. G. Parr, *Introduction to Stainless Steels*, 3rd ed., ASM International, p. 27 (1999).

2. M. L. Erbing, *Materialkunskap*, Avesta Sheffield AB, Lecture in the course *Konstruera och Arbeta i Rostfritt*, p. 1 (1998).

3. F. Falkenberg, *Initiation and Repassivation of Austenitic Stainless Steel,* Doctoral Thesis, Chalmers University of Technology, Gothenburg, Sweden, p. 1 (2000).

4. J. O. Nilsson, *Super Duplex Stainless Steel*, Mat. Sci and Tech., **8**, 685 (1992).

5. H. D. Solomon and T. M. Devine, *Duplex Stainless Steels- A Tale of Two Phases,* Duplex Stainless Steels, Conf. Proc., ASM, p. 693 (1983).

6. J. Charles, *Super Duplex Stainless Steel: structure and properties*, Duplex Stainless Steels '91, Conf. Proc., Beaune, France, p. 3 (1991).

7. R.A. Lula, *Duplex Stainless Steels*, Conf. Proc., ASM, p. iii, (1983).

8. A. J. Sedriks, *Corrosion of Stainless Steels*, John Wiley & Sons, Inc., p. 49 (1996).

9. R. Alkire and M. Verhoff, *The Bridge from Nanoscale Phenomena to Macroscopic Processes*, Electrochim. Acta, **43**, 2733 (1998).

10. P. Combrade and J.-P.Audouard, *Duplex Stainless Steels and Localized Corrosion Resistance*, Duplex Stainless Steels '91, Conf. Proc., Beaune, France, p. 257 (1991).

11. C.D.S Tuck, J.M. Sykes, and L.F. Garfias-Mesias, *The Influence of Specific Alloying Elements in the Control of Pitting Mechanisms of 25% Cr Duplex Steels*, Duplex Stainless Steels, Glasgow, 1994, paper 15.

12. L.F. Garfias-Mesias, J.M. Sykes, and C.D.S Tuck, *The Effect of Phase Compositions on the Pitting Corrosion of 25 Cr Duplex Stainless Steel in Chloride Solutions*, Corros. Sci., **38**, 1319 (1996).

13. A. P. Bond and H. J. Dundas, *Resistance of Stainless Steel to Crevice Corrosion in Seawater*, Mater. Performance, **23**, 39 (1984).

14. C. O. A. Olsson, *The Influence of Nitrogen and Molybdenum on Passive Films Formed on the Austeno-Ferritic Stainless Steel 2205 Studied by AES and XPS*, Corros. Sci., **37**, 467 (1995).

15. J. Foct, T. Magnin, P. Perrot, and J. B. Vogt, *Nitrogen Alloying of Duplex Stainless Steels*, Duplex Stainless Steels '91, Conf. Proc., Beaune, France, p. 49 (1991).

16. S. Bernhardsson, *The Corrosion Resistance of Duplex Stainless Steels*, Duplex Stainless Steels '91, Conf. Proc., Beaune, France, p.185 (1991).

17. L. Weber and P. J. Uggowitzer, *Partitioning of Chromium and Molybdenum in Super Duplex Stainless Steel with Respect to Nitrogen and Nickel Content*, Mater. Sci. Eng., A, **242**, 222 (1998).

18. R. A. Perren, T. A. Suter, P.J. Uggowitzer, L. Weber, R. Magdowski, H. Böhni, and M. O. Speidel, *Corrosion Resistance of Super Duplex Stainless Steels in Chloride Ion Containing Environments: Investigations by Means of a New Microelectrochemical Method I. Precipitation-free States,* Corros. Sci, **43**, 707 (2001).

19. L.F. Garfias-Mesias and J. M. Sykes, *Metastable Pitting in 25 Cr Duplex Stainless Steel*, Corros. Sci, **41**, 959 (1999).

20. Y. Kobayashi, S. Virtanen, and H. Böhni, *Microelectrochemical Studies on the Influence of Cr and Mo on Nucleation Events of Pitting Corrosion*, J. Electrochem. Soc., **147**, 155 (2000).

21. H. Böhni, T. Suter, and F. Assi, *Micro-electrochemical Techniques for Studies of Localized Processes in the Nanometer Range*, Surf. Coatings Tech., **130**, 80 (2000).

22. I. Annergren, *Electrochemical Impedance Spectroscopy for In-Situ Studies of Anodic Dissolution and Pitting Corrosion of Iron-Chromium Alloys*, Doctoral Thesis, Royal Institute of Technology, Stockholm, Sweden, (1996).

23. E. Bayet, F.Huet, M. Keddam, K. Ogle, and H. Takenouti, *Adaptation of the Scanning Vibrating Electrode Technique to AC Mode: Local Electrochemical Impedance Measurement*, Mater. Sci Forum, **289-292**, 57 (1998).

24. H. Uchida, M. Yamashita, S. Inoue, and K. Koterazawa, *In-situ Observations of Crack Nucleation and Growth During Stress Corrosion by Scanning Vibrating Electrode Technique*, Mater. Sci. Eng. A, **319-321**, 496 (2001).

25. D.A. Sargeant and G. I. Ronaldson, *Quantitative Measurements of Localized Corrosion Using the Scanning Reference Electrode Technique on Type 316 Stainless Steel*, Microscopy & Analysis, **52**, 21 (1996).

26. C. J. Lin, J. L. Luo, X. D. Zhuo, and Z. W. Tian, *Scanning Microelectrode Studies of Early Pitting Corrosion of 18/8 Stainless Steel*, Corrosion (Houston), **54**, 265 (1998).

27. A. Miyasaka and H. Ogawa, *In-Situ Observation of a Stainless Steel Surface in Aqueous Solutions Using Scanning Tunneling Microscope,* Corros. Sci., **31**, 99 (1990).

28. F. R. F. Fan and A. J. Bard, *In-Situ Scanning Tunneling Microscopic Study of the Corrosion of Type 304L Stainless Steel in Aqueous Chloride Media*, J. Electrochem. Soc., **136**, 166 (1989).

29. R. M. Rynders, C.-H. Paik, R. Ke, and R. C. Alkire, *Use of In-Situ Atomic Force Microscopy to Image Corrosion at Inclusions*, J. Electrochem. Soc., **141**, 1439 (1994).

30. I. Reynaud-Laporte, M. Vayer, J. P. Kauffman, and R. Erre, *An Electrochemical-AFM Study of the Initiation of the Pitting Corrosion of a Martensitic Stainless Steel*, Microsc. Mircroanal. Microstruct., **8**, 175 (1997).

31. R. E. Williford, C. F. Windisch Jr., and R. H. Jones, *In-situ Observations of the Early Stages of Localized Corrosion Using the Electrochemical Atomic Force Microscope*, Mat. Sci & Eng. A, **288**, 54 (2000).

32. L.F. Garfias-Mesias and D. J.Siconolfi, *In-situ High-Resolution Microscopy on Duplex Stainless Steels,* J. Electrochem. Soc., **147**, 2525 (2000).

33. G. Gugler, J. D. Neuvecelle, P. Mettraux, E. Rosset, and D. Landolt, *In- Situ AFM Investigation of Pitting*, The Inst. of Materials, London, Book no 577, 274 (1994).

34. H. Tanabe, K. Togashi, T. Misawa, U. Kamachi Mudali, *In-situ pH Measurements During Localised Corrosion of Type 316LN Stainless Steel Using Scanning Electrochemical Microscopy*, J. Mater. Sci. Letters, **17**, 551 (1998).

35. C. H. Paik, H. S. White, and R. C. Alkire, *Scanning Electrochemical Microscopy of Dissolved Sulfur Species from Inclusions in Stainless Steel*, J. Electrochem. Soc., **147**, 4120 (2000).

36. Y. Zhu and D. E. Williams, *Scanning Electrochemical Microscopic Observation of a Precursor State To Pitting Corrosion of Stainless Steel,* J. Electrochem. Soc., **144**, L43 (1997).

37. D. E. Williams, T. F. Mohiuddin, and Y. Zhu, *Elucidation of a Trigger Mechanism for Pitting Corrosion of Stainless Steels Using Submicron Resolution Scanning Electrochemical and Photoelectrochemical Microscopy*, J. Electrochem. Soc., **145**, 2664 (1998).

38. Y. Zhu and D. E. Williams, *Explanation for Initiation of Pitting Corrosion of Stainless Steels at Sulfide Inclusions*, J. Electrochem. Soc., **147**, 1763 (2000).

39. M. Stratmann, *The Investigation of the Corrosion Properties of Metals, Covered with Adsorbed Electrolyte Layers - A New Experimental Technique*, Corr. Sci. **27**, 869 (1987).

40. L. T. Han and F. Mansfeld, *Scanning Kelvin Probe Analysis of Welded Stainless Steel*, Corr. Sci. **39**, 199 (1997).

41. C. Chen, C. B. Breslin, and F. Mansfeld, *Scanning Kelvin Probe Analysis of the Potential Distribution under Small Drops of Electrolyte*, Mat. Sci. Forum, **289-292**, 181 (1998).

42. H. Böhni, T. Suter, and A. Schreyer, *Micro- and Nanotechniques to Study Localized Corrosion*, Electrochim. Acta, **40**, 1361 (1995).

43. S. Virtanen, A. Schreyer, and H. Böhni, *In-Situ STM and AFM Characterization of Passivity on Stainless Steels*, in Proc. 12th Int. Corr. Congr., Houston, p. 2142 (1993).

44. J. H. W. de Wit, D. H. van der Weijde, and A. J. de Jong, *Local Measurements in Electrochemistry and Corrosion Technology*, Mater. Sci Forum, **289-292**, 69 (1998).

45. E. Schmitt-Rieder, X. Q. Tong, J. P. G. Farr, and M. Aindow, *In- Situ SPM Observations of Corrosion Processes on a Duplex Stainless Steel in Saline Solutions,* in Proc. Electron Microscopy and Analysis, Birmingham, 247 (1995).

46. P. Schmutz and G. S. Frankel, *Characterization of AA2024-T3 by Scanning Kelvin Probe Force Microscopy,* J. Electrochem. Soc., **145**, 2285 (1998).

47. P. Schmutz and G. S. Frankel, *Corrosion Study of AA2024-T3 by Scanning Probe Force Microscopy and In situ Atomic Force Microscopy Scratching*, J. Electrochem. Soc., **145**, 2295 (1998).

48. V. Guillaumin, P. Schmutz, and G. S. Frankel, *Characterization of Corrosion Interfaces by the Scanning Probe Force Microscopy Technique*, J. Electrochem. Soc., **148**, B163 (2001).

49. P. Campestrini, E. P. M. Van Westing, H. W. van Rooijen, and J. H. W. de Wit, *Relation Between Microstructural Aspects of AA2024 and its Corrosion Behaviour Investigated Using AFM Scanning Potential Technique*, Corros. Sci., **42**, 1853 (2000).

50. H. Masuda, *Effect of Magnesium Chloride Liquid Thickness on Atmospheric Corrosion of Pure Iron*, Corrosion *(Houston)*, **57**, 99 (2001).

51. *Sandvik Steel Corrosion Handbook-Stainless Steels*, AB Sandvik Steel and Avesta Sheffield AB, p. 16 (1994).

52. D. A. Jones, *Principles and Prevention of Corrosion*, Macmillan Publishing Company, p. 125 (1992).

53. J. Castle, *Survey of SPM Methods and their Comparison with other Microscopical Techniques*, Lecture 1 in the course *Scanning Probe Microscopy: Principles and Practice*, University of Surrey, 18-22 January 1999.

54. R. Guckenberger, *STM*, in R. J. Colton, A. Engel, J. E. Frommer, H. E. Gaub, A. A. Gewirth, R. Guckenberger, W. M. Heckl, B. Parkinson, J. Rabe, Editors, *Procedures in Scanning Probe Microscopes*, Wiley & Sons, p. 50 (1998).

55. P.A. Christensen and A. Hamnett, *Techniques and Mechanisms in Electrochemistry.* Blackie Academic & Professional, p. 67 (1994).

56. M. Virkin, *High Resolution Studies of Heterogeneous Processes with the Scanning Electrochemical Microscope*, Mikrochimica Acta, **130**, 127 (1999).

57. J. Wittborn, *Nanoscale Studies of Functional Materials using Scanning Probe Microscopy*, Doctoral Thesis. Royal Institute of Technology, Stockholm, Sweden, p. 10 (2000).

58. A. Dias and M. S. Andrade, *Atomic Force and Magnetic Force Microscopies Applied to Duplex Stainless Steels*, Appl. Surf. Sci., **161**, 109 (2000).

59. B. R. A. Neves and M. S. Andrade, *Identification of two Patterns in Magnetic Force Microscopy of Shape Memory Alloys*, Appl. Phys. Lett., **74**, 2090 (1999).

60. C. Chen and F. Mansfeld, *Potential Distribution in the Evans Drop Experiment,* Corr. Sci. **39**, 409 (1997).

61. M. Stratmann and H. Streckel, *On the Atmospheric Corrosion of Metals which are Covered with Thin Electrolyte Layers- I. Verification of the Experimental Technique*, Corros. Sci., **30**, 681 (1990).

62. M. Stratmann and H. Streckel, *On the Atmospheric Corrosion of Metals which are Covered with Thin Electrolyte Layers-II. Experimental Results*, Corros. Sci., **30**, 697 (1990).

63. M. Stratmann and H. Streckel, *On the Atmospheric Corrosion of Metals which are Covered with Thin Electrolyte Layers-III. The Measurement of Polarisation Curves on Metal Surfaces which are Covered by Thin Electrolyte Layers*, Corros. Sci., **30**, 715 (1990).

64. H. O. Jacobs, H. F. Knapp, S. Müller, and A. Stemmer, *Surface Potential Mapping: A Qualitative Material Contrast in SPM*, Ultramicroscopy, **69**, 39 (1997).

65. H. O. Jacobs, H. F. Knapp, and A. Stemmer, *Practical Aspects of Kelvin Probe Force Microscopy*, Rev. Sci. Instrum., **70**, 1756 (1999).

66. M. P. Seah and D. Briggs, *A Perspective on the Analysis of Surfaces and Interfaces*, Chapter 1 in *Practical Surface Analysis*, 2nd Edition, M. P. Seah and D. Briggs Editors, John Wiley & Sons, New York, USA, p. 5 (1990).

67. S. Mischler, H. J. Mathieu, and D. Landolt, *Investigation of a Passive Film on an Iron-Chromium Alloy by AES and XPS*, Surf. Interface. Anal., **11**, 182 (1998).

68. R. F. A. Jargelius-Pettersson, *The Influence of N, Mo and Mn on the Microstructure and Corrosion Resistance of Austenitic Stainless Steels*, Doctoral Thesis, Royal Institute of Technology, Stockholm, Sweden, p. 10 (1998).

69. R. Qvarfort, *Transpassive Corrosion of High Alloy Stainless Steels. Part 2: Investigations of the Secondary Transpassive Range*, CITU Hda Research Report 1998/003-R, ISSN 1401-5935 p. 10 (1998).

70. E. Schmitt-Rieder, M. Ashworth, and J. P. G. Farr, *The Effect of Nitrogen on the Stability of the Passive Film on a Zeron 100 Super Duplex Stainless Steel*, Electrochem. Solid-State Lett., **2**, 19 (1999).

71. J. W. Schultze and M. Schweinsberg, *From pm to Km: Scaling Up and Scaling Down of Electrochemical Systems with TiO_2 and ZrO_2 Passive Films as an Example*, Electrochim. Acta, **43**, 2761 (1998).

72. E. Symniotis, *Galvanic Effects on the Active Dissolution of Duplex Stainless Steels*, Corrosion (Houston), **46**, 2 (1990).

73. E. Symniotis, *The Influence of the Phase-Area Ratio and Microstructure on the Dissolution Rate of Duplex Stainless Steels in Acids*, in Proc. 11th Int. Corr. Congr., Florence, p. 5.203 (1990).

74. E. Symniotis, *Dissolution Mechanism of Duplex Stainless Steels in the Active-to-Passive Transition Range and the Role of Microstructure*, Corrosion (Houston), **51**, 8 (1995).

75. S. Hertzman, W. Roberts, and M. Lindenmo, *Microstructure and Properties of Nitrogen Alloyed Duplex Stainless Steel After Welding*, in Proceedings of the DSS conference, The Hague, Netherlands, p. 257 (1986).

76. Y. C. Lu, M. B. Ives, and C. R. Clayton, *Synergism of Alloying Elements and Pitting Corrosion Resistance of Stainless Stainless Steels*, Corros. Sci, **35**, 89 (1993).

77. G. P. Halada, D. Kim, and C. R. Clayton, *Influence of Nitrogen on Electrochemical Passivation of High-Nickel Stainless Steels and Thin Molybdenum-Nickel Films,* Corrosion (Houston), **52**, 36 (1996).

78. I. Olefjord and C. R. Clayton, *Surface Composition of Stainless Steel during Active Dissolution and Passivation,* ISIJ International, **31**, 134 (1991).

79. L. Wegrelius and I. Olefjord, *Dissolution and Passivation of Stainless Steels Exposed to Hydrochloric Acid,* Mater. Sci Forum, **185-188**, 347 (1995).

80. L. Wegrelius and I. Olefjord, *Influence of N on Passivation of Stainless Steels,* Corros. Sci, **38,** 1203 (1996).

81. A. J. Sedriks, *Corrosion of Stainless Steels*, John Wiley & Sons, Inc., p. 142 (1996).

82. M. Femenia, J. Pan, C. Leygraf, and P. Luukkonen, *In Situ Study of Selective Dissolution of Duplex Stainless Steel 2205 by Electrochemical Scanning Tunnelling Microscopy* , Corrosion Science, **43**, 1939 (2001).

83. J. Pan, M. Femenia, and C. Leygraf, *Corrosion Behavior of a Duplex Stainless Steel Studied by STM/AFM Based Scanning Electrochemical Microscopy*, in *Localized In Situ Methods for Investigating Electrochemical Interfaces*, S. R. Taylor, A. C. Hillier, and M. Seo, Editors, PV 99-28 p. 131, The Electrochemical Society Proceedings Series, Pennington, NJ (1999).

84. M. Femenia, J. Pan, and C. Leygraf, *In Situ Local Dissolution of Duplex Stainless Steels in 1M H_2SO_4+ 1M NaCl by Electrochemical Scanning Tunneling Microscopy,* Journal of The Electrochemical Society, **149**, B187 (2002).

85. M. Femenia, C. Canalias, J. Pan, and C. Leygraf, *Scanning Kelvin Probe Force Microscopy and Magnetic Force Microscopy for Characterization of Duplex Stainless Steels,* Journal of The Electrochemical Society, *in press*.

86. M. Femenia, J. Pan, and C. Leygraf, Characterization of Ferrite-Austenite Boundary Region of Duplex Stainless Steels by Scanning Auger Electron Spectroscopy, Manuscript to be submitted.